



CHALMERS
UNIVERSITY OF TECHNOLOGY

Comparison of solids conveying mechanisms in fluidized bed systems – Alternatives to riser

Downloaded from: <https://research.chalmers.se>, 2025-07-01 19:49 UTC

Citation for the original published paper (version of record):

Farha, M., Guio Perez, D., Johnsson, F. et al (2025). Comparison of solids conveying mechanisms in fluidized bed systems – Alternatives to riser. *Chemical Engineering Science*, 317.
<http://dx.doi.org/10.1016/j.ces.2025.122000>

N.B. When citing this work, cite the original published paper.



Comparison of solids conveying mechanisms in fluidized bed systems – Alternatives to riser

Munavara Farha ^{*} , Diana Carolina Guío-Pérez , Filip Johnsson, David Pallarès 

Department of Space, Earth and Environment, Division of Energy Technology, Chalmers University of Technology, Hörsalsvägen 7B, 412 96 Gothenburg, Sweden

ARTICLE INFO

Keywords:

Fluidization
Bubbling fluidized bed
Fluid-dynamical scaling
Solids convective transport
Fluidized bed system

ABSTRACT

The macroscopic convective transport of solids in fluidized bed systems is vital for efficient heat and mass transfer in solids-looping and solids-throughput processes. While risers are a conventional setup to promote solids convection, emerging applications demand higher solids flux and more compact, energy-efficient alternatives. This study investigates five solids conveying mechanisms in a fluid-dynamically down-scaled cold flow model using Geldart B-type solids. The system features a closed circulation loop, interconnecting a bubbling bed with a conveying module that induces net horizontal solids crossflow.

Each conveying strategy is driven by a distinct mechanism: (i) *Free solids splashing* relies on bubble bursts at the bed surface to eject particles; (ii) *Confined solids splashing* amplifies this effect within a narrow geometry through turbulent interactions to enhance particle lift; (iii) *Slugging* induces transport via the rise and collapse of gas slugs in vertical ducts; (iv) *Solids entrainment* achieves lift by elutriating particles from the dense bed through high gas velocities; and (v) *Directed gas injection* imparts lateral momentum via angled nozzles.

The solids flow rate is measured using magnetic solids tracing technique. Conveying efficiency is assessed by comparing energy imparted to solids with energy input from fluidization gas. *Free solids splashing* and *directed gas injection* achieve the highest upscaled transport rates (5×10^{-2} – 2×10^3 kg/m²·s) at gas velocities of 1.9–4.3 m/s, outperforming conventional risers. *Free solids splashing* also offers the highest energy efficiency, while *slugging* and *directed gas injection* offer intermediate performance. *Confined solids splashing* and *solids entrainment* show the lowest efficiency.

1. Introduction

The macroscopic convective transport of solids within fluidized bed systems is essential for the efficient transfer of mass and energy across various reactors or reaction zones, ensuring optimal interaction between gas and solid phases. This feature is particularly important in processes that involve solids cycling, such as biomass indirect pyrolysis/gasification, chemical/calcium looping, and catalytic cracking, as well as in solids throughput applications like drying and iron reduction (Grace et al., 2020; Kunii and Levenspiel, 1991). Traditionally, the flow of solids in these systems has been forced by pneumatic transport mechanisms, typically through riser configurations. An example of this is found in dual fluidized bed (DFB) systems, which are integral to processes employing solids cycling, such as chemical synthesis, cracking, and biomass conversion, due to their effectiveness in achieving controlled mass and energy transfer between reactors (Kunii and Levenspiel, 1991). A key characteristic among current DFB configurations is the

incorporation of at least one riser (also called circulating fluidized bed, CFB) whose particle elutriation drives the solids circulation rate in the system. Such a CFB is combined with the second bed reactor, which can be either a second CFB or a bubbling fluidized bed (BFB) (Kunii and Levenspiel, 1991). However, incorporating a CFB to induce convective transport introduces design requirements, such as a large riser vertical dimension (proportional to the solids throughput) and higher energy demand due to the increased gas velocities required compared to bubbling beds. Both factors are pivotal for process performance (Grace et al., 2020; Kunii and Levenspiel, 1991). Thus, new applications requiring higher solids circulation rates may benefit from alternative fluidized bed designs that explore non-conventional configurations for inducing and controlling the macroscopic solids flow, offering more compact designs and improved energy efficiency.

Within the field of fluidization technology, various potential configurations have been explored and shown capable of achieving net solids transport. These configurations have been designed and operated with the aim of exploiting the characteristics of specific fluidization

* Corresponding author.

E-mail address: m.farha@chalmers.se (M. Farha).

Nomenclature			
A	Cross-sectional area [m ²]	Re_p	Particle Reynolds number [-]
Ar	Archimedes number [-]	t	Time [s]
C	Concentration [kg/m ³]	u_0	Fluidization velocity [m/s]
D_s	Solids lateral dispersion coefficient [m ² /s]	u_{mf}	Minimum fluidization velocity [m/s]
D_t	Tube diameter [m]	u_{ms}	Minimum slugging velocity [m/s]
d_{32}	Sauter mean diameter [μ m]	u_{mt}	Transition velocity to turbulent fluidization regime [m/s]
d_p	Mean particle diameter [μ m]	u_s	Solids velocity [m/s]
E	Energy flux [J/s]	x	Horizontal position [m]
g	Gravity constant, 9.81 [m/s ²]	<i>Greek letters:</i>	
H	Settled bed height [m]	γ	Isentropic expansion factor [-]
H_{mf}	Bed height at minimum fluidization [m]	ε_s	Solids volume fraction [-]
L	Length [m]	η	Solids conveying efficiency [-]
\dot{m}_s	Solids mass flowrate [kg/s]	μ_f	Gas viscosity [Pa•s]
P	Pressure [Pa]	ρ_b	Bulk density [kg/m ³]
Q	Volumetric flowrate of gas [m ³ /s]	ρ_f	Gas density [kg/m ³]
		ρ_s	Solids density [kg/m ³]

regimes. In short, fluidization regimes categorize the distinct states observed when a fluid (liquid or gas) flows through a bed of granular material at varying velocities (Grace et al., 2020; Kunii and Levenspiel, 1991). The transition between these regimes is primarily influenced by the gas velocity and the properties of the gas and the solids. For Geldart B solids, increasing the gas velocity beyond *minimum fluidization* shifts the system into the *bubbling regime*, which is distinguished by the presence of rising gas bubbles whose size (and thus the magnitude of pressure fluctuations) increases with fluidization velocity. For beds with a high aspect (height-to-width) ratio, as gas bubbles grow with height the system can evolve into the *slugging regime*, which is characterized by the formation of gas pockets that span the entire cross-section, yielding the rise (and sometimes even the collapse) of solids packets. With a higher fluidization velocity, the system eventually enters the *turbulent fluidization regime*, where individual bubbles become indistinguishable, resulting in a highly mixed state with intense particle-gas interactions and reduced pressure fluctuations. However, the exact boundaries of this regime are often disputed, as it is not universally defined and can vary depending on the system's scale and design (Bi et al., 2000). Increasing the gas velocity beyond this regime yields states (*fast bed regime*, *pneumatic regime*) where the solids upward entrainment by the gas is significant, establishing circulating conditions.

Literature covers solids circulation in fluidized bed systems, with vertical circulation in CFBs and DFBs being well-studied, while horizontal circulation is far less explored. The summary below categorizes solids conveying configurations into four types: BFB-BFB (horizontal), compartmentalized BFB (horizontal), BFB-CFB (vertical), and slugging (vertical). Further, the influence of gas injection on achieved solids flow rate is also highlighted, as nozzle design and placement play a crucial role in controlling solids transport and mixing within fluidized bed systems.

Regarding BFB-BFB configurations aimed at transporting solids between distinct bed reactors, Adánez et al. (Adánez et al., 2006) implemented solids transport in their chemical looping combustion system by integrating interconnected BFB reactors, utilizing a pressure difference created by the distinct fluidization conditions. This setup, when combined with a loop-seal system and a solids valve, facilitates a controlled overflow of partially reduced oxygen carrier particles from the fuel reactor into a U-shaped fluidized loop seal, with subsequent transfer of the solids to the air reactor.

Compartmentalized BFBs are designed to circulate particles across different compartments within a single bed container (Kuramoto et al., 1986; Snip, 1996; Foscolo et al., 2007; Reichhold and Hofbauer, 1995; Rubio et al., 2004). Kuramoto et al. (Kuramoto et al., 1986) studied solids transport in a two-dimensional fluidized bed divided by a

partition with an opening, creating two sections with different superficial gas velocities. They found that the solids circulation rate between these sections was influenced by the gas velocity in the high-velocity upward-flowing bed section and the opening-to-downcomer area ratio, enabling an effective control of net solids transport by adjusting these parameters. Snip et al. (Snip, 1996) described an Interconnected Fluidized Bed (IFB) reactor technology that is characterized by multiple dense-bed and lean-bed sections. Solids transport occurs through consecutive compartments with alternating aeration velocities, such that high-velocity fluidization causes the solids to splash over a weir, while low-velocity aeration facilitates their flow through an orifice. A similar design study was conducted by Foscolo et al. (Foscolo et al., 2007), in which the solids circulation in an IFB gasifier was driven by a pressure difference across two fluidized beds that are separated by a partition plate. Reichhold et al. (Reichhold and Hofbauer, 1995) developed an internally circulating fluidized bed (ICFB) system featuring two adjacent bubbling fluidized beds separated by a partition with horizontal openings. This arrangement, when combined with the use of varying fluidization rates, allowed for controlled circulation of the bed material between the two sections. Rubio et al. (Rubio et al., 2004) achieved controlled circulation of solids in an ICFB system by creating a pressure difference between two zones of different bed porosities separated by a vertical partition with an orifice of adjustable size.

The use of a CFB is a common practice to induce solids flow in fluidized bed systems. In this setup, a riser (a bed operated at fluidization velocities beyond the turbulent regime to achieve significant solids entrainment from the bottom region) drives the convective transport. Many examples of such configurations are found in the literature. Linderholm et al. (Linderholm et al., 2008) utilized a CLC reactor system in which the gas velocity in the air reactor (the riser) drives the circulation of particles between this bed and the other one, a bubbling bed acting as the fuel reactor. Solids are entrained in the gas flow, separated in a cyclone, and returned to the bubbling fuel reactor via a downcomer, together constituting a mechanism for continuous and controlled transport of solids. Xu et al. (Xu et al., 2009) devised a system that integrates a pneumatic riser combustor and a two-staged fluidized bed reactor. The lower stage served as a bubbling bed gasifier, while the upper stage, designed with an expanded cross-section, enhanced the gas residence time and curtailed fuel particle elutriation. An overflow pipe was used for interstage particle transfer, ensuring precise control of particle circulation. Charitos et al. (Charitos et al., 2010) examined a cold model of a DFB system, in which the riser features an "abrupt" inclined exit. The system was completed by a double exit loop seal with an adjustable orifice for controlling the solids circulation rate, and a BFB. In the DFB system investigated by Hawthorne et al. (Hawthorne

et al., 2012), solids transfer between the CFB regenerator and the BFB gasifier was attained through an L-valve and a hydraulic connection. This configuration enables controlled particle entrainment and circulation, ensuring effective material exchange between the two reactors. Nguyen et al. (Nguyen et al., 2012) utilized a configuration that integrates a BFB gasifier with a riser, connected by a loop seal. This setup enabled an efficient integration of the gasification and combustion processes, with the riser facilitating continuous particle transport. Bao et al. (Bao et al., 2013) designed a dual BFB reactor system, in which a riser transports solids between a fuel reactor (FR) and an air reactor (AR), using a cyclone for gas-solids separation. Secondary air was introduced at the top of the AR to enhance particle entrainment, and U-shaped loop seals were used to prevent gas leakages between the reactors, ensuring effective circulation of the particles. Li et al. (Li et al., 2018) have described an indirect steam gasification setup that utilizes a BFB-CFB arrangement. Parameters such as the aeration flowrate, nozzle placements, and pressure variances exert substantial influences over the solids circulation rate. Their results indicate that beyond some point, higher gas velocities in the riser result in diminished solids circulation rates due to decreased solids concentration, while increased pressure drop substantially enhances solid circulation flux. In a similar configuration, Luo et al. (Luo et al., 2019) investigated the solids transport dynamics between a fast fluidized bed and a BFB, controlling the solids circulation rate through adjustments in the system's solid inventory. Their findings indicate that both the solids circulation rate and fluctuations thereof increase with increased solids inventory, presenting challenges in relation to operational stability.

Slugging has also been investigated as basis for alternative configurations to attempt convective transport of solids. In most fluidized bed operations, slugging is a phenomenon that typically needs to be avoided due to its potential to disrupt steady state conditions, reducing the gas-solids contact, leading to uneven temperature profiles, and causing mechanical wear or damage to the reactor internals (Grace et al., 2020; Kunii and Levenspiel, 1991). Despite these challenges, slugging can have specific applications in advanced designs and may support solids transport in the dense phase. For instance, Fan et al. (Fan and Toda, 1983) introduced the Multi-Solid Pneumatic Transport Bed (MPTB), a reactor with a bimodal solids size distribution where fine particles follow the flow pattern of a circulating fluidized bed, while coarse particles establish a dense bed that operates either in turbulent or slugging mode. It operates by ensuring the gas velocity through the bed is greater than the terminal velocity of the circulating particles but less than that of the dense particles, thereby enabling the effective transport of solid. The slugging regime in interconnected fluidized beds has been the focus of a limited number of research efforts. Foscolo et al. (Foscolo et al., 2007) observed in a sectionized BFB that slugging, occurring in the up-flowing bed (UFB) section at a fluidizing velocity of around $3u_{mf}$, enhances the vertical distribution of biomass fuel, thus counteracting its segregation at the bed surface. This results in more uniform and rapid heating of fuel particles, reducing fine particle elutriation, and consequently improving the yield and quality of the product gas. Luo et al. (Luo et al., 2020) observed slugging specifically in the riser section of a DFB gasifier by assessing the bubble characteristics. The authors noted that the slugging flow regime exhibited larger and more numerous bubbles, which led to an enhanced upward transport of the particles compared to the bubbling regime.

Gas injection has also been observed to impact the flow patterns of solids in fluidized beds. In particular, the design of nozzles has received attention due to its potential to influence the transport and mixing of solids across different types of fluidized bed systems. Dawe et al. (Dawe et al., 2008) explored the dynamics of sonic gas jets in a 2.5D gas-solids fluidized bed system, demonstrating how nozzle geometry and gas flowrate influence the penetration depth and expansion angle of the gas jets, and thereby the solids transport and distribution within the reactors. In their study of a DFB system, Fang et al. (Fang et al., 2009) highlighted the critical roles of solid injection nozzle design and

placement in governing material transport between reactors. Kaewluan et al. (Kaewluan and Pipatmanomai, 2011) investigated a BFB gasifier, implementing a nozzle-type air distributor that was designed for optimal gas and solid recirculation while preventing bed aggregation. Youn et al. (Youn et al., 2022) detailed an experimental CFB system that incorporates what the authors refer to as a 'fast fluidized bed' riser, along with upper/lower bubbling beds, and a U-bend loopseal. Aeration nozzles are positioned at specific locations to regulate the solids flow from the lower BFB to the riser, emphasizing the controlled movement of solids. Werner et al. (Werner et al., 2023) studied gas injection in a cylindrical gas-fluidized bed using a nozzle-type distributor, focusing on the impacts of orifice angles on fluidization and flow patterns. The study highlights that nozzles with horizontal or near-horizontal outlets are highly effective for achieving consistent and rapid solids recirculation, indicating the potential for controlled solids transport.

Overall, the literature presents various examples of configurations designed to induce macroscopic solids circulation in fluidized bed systems, demonstrating a wide range of fluidization regimes, conditions, and designs. However, the above review reveals that a systematic assessment and comparison of solids conveying mechanisms' performance has yet to be conducted.

The aim of this work is to examine methods for inducing macroscopic convective transport of solids in fluidized bed systems. Specifically, the objective is to evaluate various solids conveying configurations—alternative to the conventional riser—in terms of efficiency, controllability, and flexibility. Five distinct mechanisms are investigated, each based on a different principle: free solids splashing, confined solids splashing, slugging, solids entrainment, and directed gas injection. The novelty of this work lies in the systematic and quantitative comparison of these alternative conveying mechanisms, providing new insights into their potential for enabling more compact and energy-efficient fluidized bed designs. The investigation is performed in a fluid-dynamically down-scaled cold-flow model. The solids mass flow rate is measured using the magnetic solids tracing (MST) technique, which—combined with horizontal pressure drop measurements—allows for evaluation of solids conveying efficiency. The scope of this study is limited to systems operating with Geldart group B-type solids.

2. Theory and methodology

2.1. Experimental setup

This work applies a cold flow model using Glicksman's simplified set of scaling laws (Glicksman, 1988; Glicksman et al., 1993) to replicate the fluid dynamics of typical fluidized bed processes for thermochemical conversion. Fluid-dynamic scaling, based on the chosen set of laws, is a validated method (Glicksman et al., 1993; Mirek, 2016; Djerf et al., 2021) that enables the study of gas-solid flows in large systems operating at high temperatures and/or pressures by reproducing their behavior in small-scale, room-temperature systems. Cold-flow models offer design flexibility, simplified diagnostics, and safer, more cost-effective experimentation.

The cold flow model used (see top view in Fig. 1a and isometric view in Fig. 1b) is designed as a closed-loop circuit in which Geldart B-type solids, fluidized under bubbling conditions, are transported horizontally. The unit features in its center a rectangular section (hereinafter referred to as the *centre box*) which creates a closed loop. The transport of solids occurs in the clockwise direction around this centre box. A specific segment of the loop is designated for the placement of the different solids conveying configurations to be assessed (referred to as the *conveying zone* or *CZ*). The air supply to this conveying zone is controlled independently of the fluidization air flow supplied to the rest of the loop (referred to as the *transport zone*, or *TZ*), which is maintained under bubbling conditions at a fluidization number (u_0/u_{mf}) of 3. For further schematic details of the experimental setup, see Appendix A.

Table 1 provides the fluid-dynamic scaling of the main parameters,

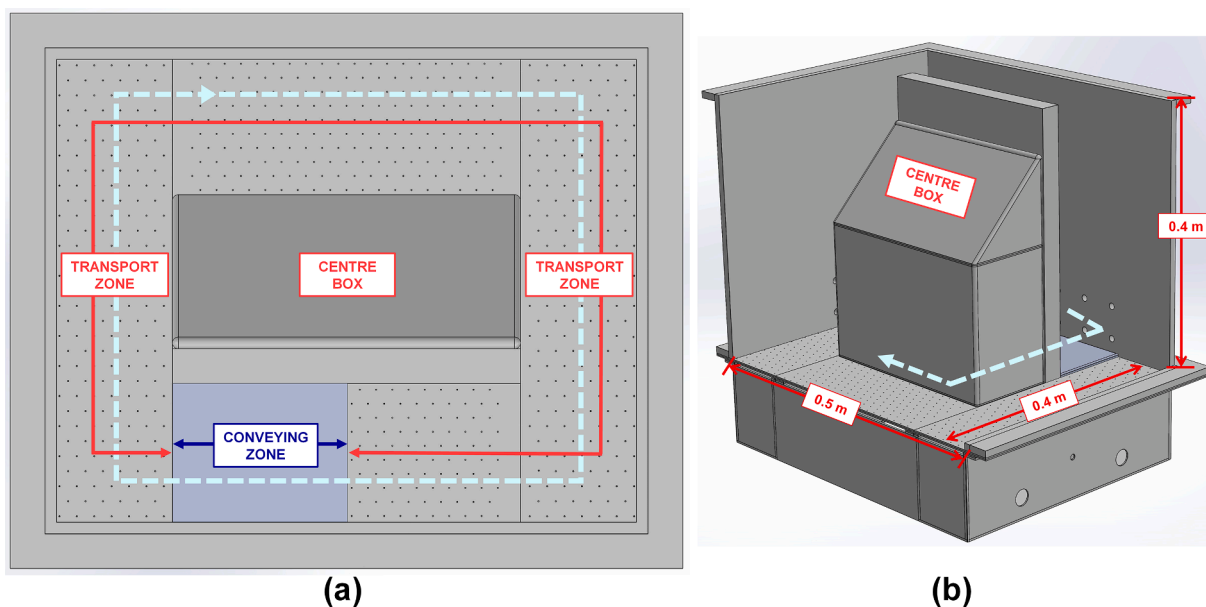


Fig. 1. Fluid-dynamically down-scaled cold flow model used for the experiments, shown in (a) top view and (b) isometric view. A flow of solids (moving clockwise) is forced in the conveying zone, where a solids conveying configuration is inserted.

Table 1

Main parameters used in the fluid-dynamically scaled model.

Parameter	Unit	Hot unit	Cold model
Bed geometry	m	L_{HOT}	$0.12 \cdot L_{HOT}$
Temperature	°C	800	24
Fluidization gas	–	Air or flue gases	Air
Gas density (ρ_f)	kg/m ³	0.359	1.187
Gas viscosity (μ_f)	m ² /s	1.4×10^{-4}	1.54×10^{-5}
Minimum fluidization velocity (u_{mf})	m/s	0.31	0.108
Bed material	–	Silica sand	Bronze
Particle density (ρ_s)	kg/m ³	2650	8770
Mean particle diameter (d_p)	µm	950	125
Gas superficial velocity (u_0)	m/s	$u_{0,HOT}$	$\sqrt{0.12} u_{0,HOT}$
Minimum fluidization velocity (u_{mf})	m/s	0.31	0.108
Horizontal solids mean velocity (u_s)	m/s	$u_{s,HOT}$	$0.347 \cdot u_{s,HOT}$
Solids lateral dispersion coefficient (D_s)	m ² /s	$D_{s,HOT}$	$0.042 \cdot D_{s,HOT}$

including the operational conditions and bed materials used in both the cold flow model and the large-scale hot unit being reproduced—a fluidized bed for thermochemical conversion where silica sand is fluidized with air or flue gases at 800 °C. As shown, scaling based on Glicksman’s simplified set of scaling laws (Glicksman, 1988; Glicksman et al., 1993) yields a length scaling factor of 0.12 (Farha et al., 2023). Accordingly, the experimental unit has a total width of 0.5 m, depth of 0.4 m and height of 0.5 m. The loop for the horizontal transport of solids has a length of 1.24 m (equivalent to 10.35 m on an up-scaled basis). Note that the hot unit mentioned in this work represents a reference large-scale framework for envisioned applications involving Geldart B solids under hot conditions, rather than representing an existing facility.

2.2. Solids conveying mechanisms

The various solids conveying mechanisms studied in this work are designed based on the principles behind different fluidization regimes, aiming to exploit their respective governing factors. Fig. 2 shows the solids conveying configurations examined in this study: (a) Free solids splashing; (b) Confined solids splashing; (c) Slugging; (d) Solids entrainment; and (e) Directed gas injection.

2.2.1. Free solids splashing

This configuration (Fig. 2a), designed to operate under the bubbling regime (Grace et al., 2020), seeks to exploit the fact that gas bubbles drag solids upward in their wakes as they rise in the dense bed. Upon bursting at the bed surface, these bubbles expel solids into the freeboard in a phenomenon known as splashing (Grace et al., 2020; Zenz and Othmer, 1960; Davidson et al., 1985). This splashing event is characterized by brief, localized increases in the gas and solids velocities at the surface of the dense bed, resulting in a high flux of solids being ejected (Djerf et al., 2021). The ejected solids display a wide range of velocities and ejection angles, eventually forming a ballistic backmixing pattern (Santana et al., 2005).

To facilitate solids conveyance, the system employs a confined conveying area, enclosed by both a barrier threshold—extending from the bottom plate to the dense bed surface—and a partially immersed hanging wall. A gap above the gas nozzle allows solids to enter the conveying area. The confined area is fluidized at a gas velocity sufficient to induce significant solids splashing, propelling a portion of the splashed solids over the threshold and thereby generating a horizontal net solids flow. An inclined surface is affixed to direct the trajectory of splashing solids, thereby enhancing overall solids conveyance. The threshold prevents solids from backmixing into the conveying zone, either through mixing within the dense bed or back-splashing.

2.2.2. Confined solids splashing

This configuration (Fig. 2b) utilizes the solids splashing occurring just above the dense bed surface, similar to the free solids splashing setup described earlier, but with a much smaller space between the threshold and the hanging wall. In other words, the geometry of the conveying section is strongly confined in the horizontal direction. This allows operation at higher superficial gas velocities, covering not only the bubbling but also the turbulent fluidization regimes, thus including the point of maximum pressure fluctuation. In the turbulent regime, gas bubbles persist to some extent, but they are less well-defined and irregularly shaped compared to those in the bubbling regime. This results in an increase in the kinetic energy introduced by the gas phase, resulting in chaotic and intense particle movement that can be exploited to induce forced convective transport through vigorous solids splashing (Grace et al., 2020; Davidson et al., 1985).

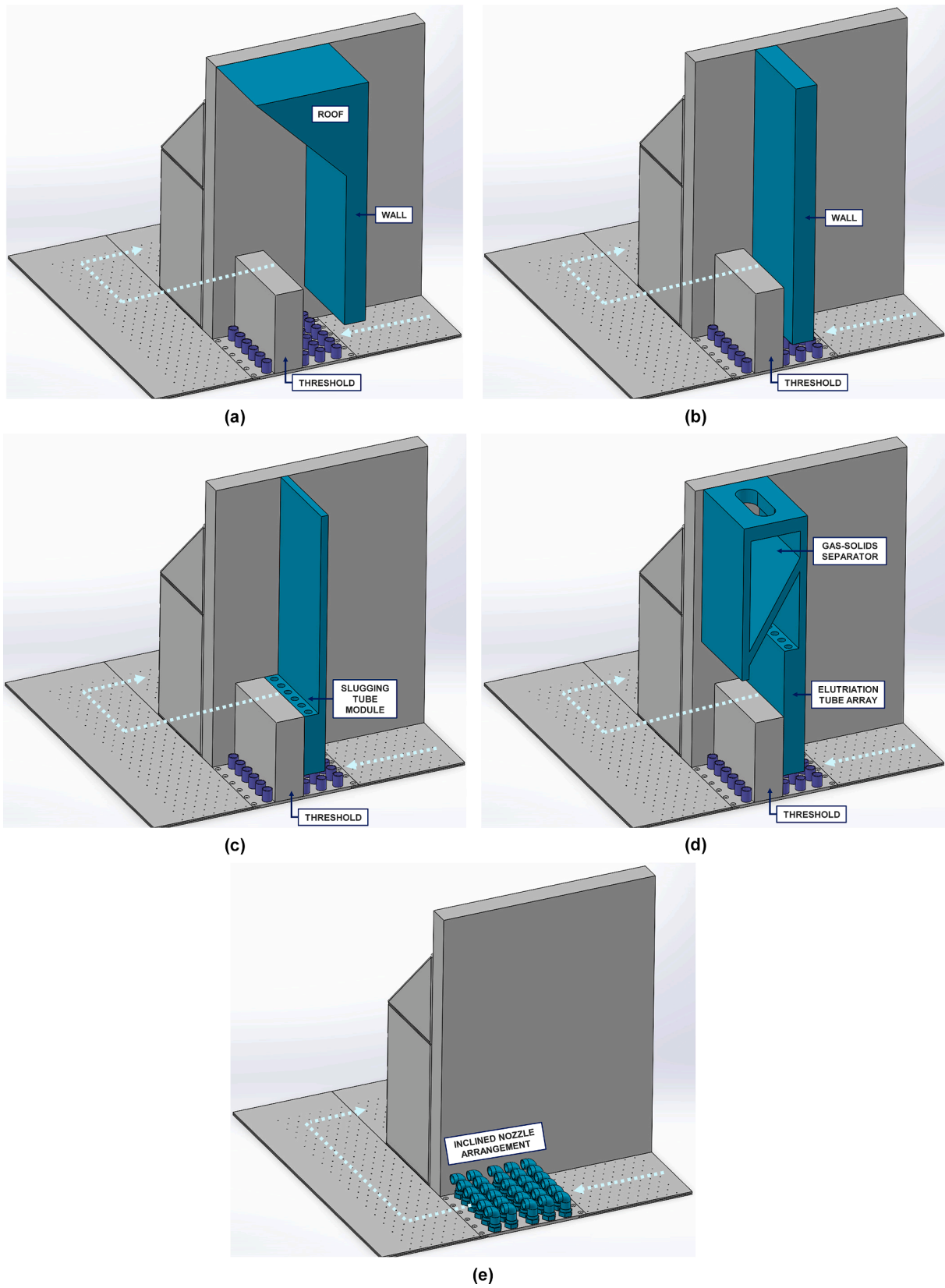


Fig. 2. Solids conveying configurations studied: (a) Free solids splashing, (b) Confined solids splashing, (c) Slugging, (d) Solids entrainment, and (e) Directed gas injection.

2.2.3. Slugging

This configuration (Fig. 2c) aims to utilize the potential of rising solids slugs, driven by gas drag, to achieve vertical transport of solids. These slugs induce a pronounced pulsating flow pattern of the solids, and upon collapsing, create a solids recirculation pattern within the bed (Grace et al., 2020; Davidson et al., 1985; Leva, 1959). The module comprises of six thin vertical ducts, with their lower ends positioned a few centimeters above the fluidization plate and their upper ends extending slightly above the bed height of the transport zone. The small diameter and high fluidization velocity are designed to promote slug formation within each duct. A threshold, similar to that used in the previous configuration, is included to prevent backmixing of the conveyed solids.

2.2.4. Solids entrainment

This configuration (Fig. 2d) exploits the phenomenon of solids entrainment as the transport mechanism. Entrainment, which occurs when relatively dispersed solids are vertically transported by the gas stream, is a phenomenon that can be observed in various fluidization regimes (particularly in fast fluidization and pneumatic regimes) and intensifies notably with increased gas velocity (Grace et al., 2020; Kunii and Levenspiel, 1991). The use of gas velocities exceeding the terminal velocity of the solids blurs the distinction between the dense and dilute solids regions. In this regime, the gas phase flows predominantly as jet streams and throughflow, rather than in clearly defined bubbles (Grace et al., 2020; Kunii and Levenspiel, 1991; Davidson et al., 1985), leading to significant drag of the solids by the gas stream. In closed circulation systems, the solids elutriated from the riser necessitate the use of solids separation devices, such as cyclones (Grace et al., 2020; Kunii and Levenspiel, 1991; Davidson et al., 1985), along with a feedback arrangement. To induce solids entrainment, the module features ducts similar to those in the slugging configuration but taller and with a restricted cross-sectional area to achieve higher gas velocities. Additionally, a gas-solids separator ensures continuous solids flow by directing entrained and separated solids into the transport section.

2.2.5. Directed gas injection

In this configuration (Fig. 2e), inclined nozzles are used to inject the fluidizing gas in the conveying zone. This design introduces a horizontal component to the trajectory of gas bubbles, which in turn imparts a net horizontal velocity to the solids dragged in the bubble wakes (Klinzing et al., 2010; Hilgraf and Hilgraf, 2024).

2.3. Measurement of the solids flowrate

The cold flow model is instrumented with magnetic solids tracing (MST) coils (Guío-Pérez et al., 2017), tailored to evaluate the solids flowrate under different operational conditions. The MST technique measures the change in the impedance of a coil when a magnetic material enters its magnetic field, with signal strength proportional to the concentration of magnetic material within the sensed volume. Fig. 3a shows a schematic of the experimental setup; the cross-section used to measure the solids flowrate is highlighted and marked as the 'measuring zone'. An example of a typical transient concentration profile obtained from the measurements is presented in Fig. 3b. By positioning MST coils at various points along the solids pathway, the peak injection of tracer solids can be accurately tracked, and the resulting transient signals are used to determine the mean horizontal velocity of the solids flow (Guío-Pérez et al., 2017; Farha et al., 2024). As illustrated in Fig. 3a, four coils are placed sequentially along the solids flow direction, spaced 0.05 m apart. The coils have a rectangular shape and frame the cross-sectional area of the channel. The coils are as wide as the channel and have a height sufficient to ensure that the magnetic field covers the range of bed heights used in the study.

The measurement procedure is initiated by the introduction of a small batch of tracer material 0.14 m upstream of the first coil. The batch of tracer material corresponds to 200 g of ferromagnetic powder (representing roughly only 0.3 % of the total solids mass) with a magnetic susceptibility of 0.9. This tracer material is chosen to have fluid-dynamical properties similar to the bed solids, to mimic accurately the flow pattern. It is injected homogeneously across the entire bed height

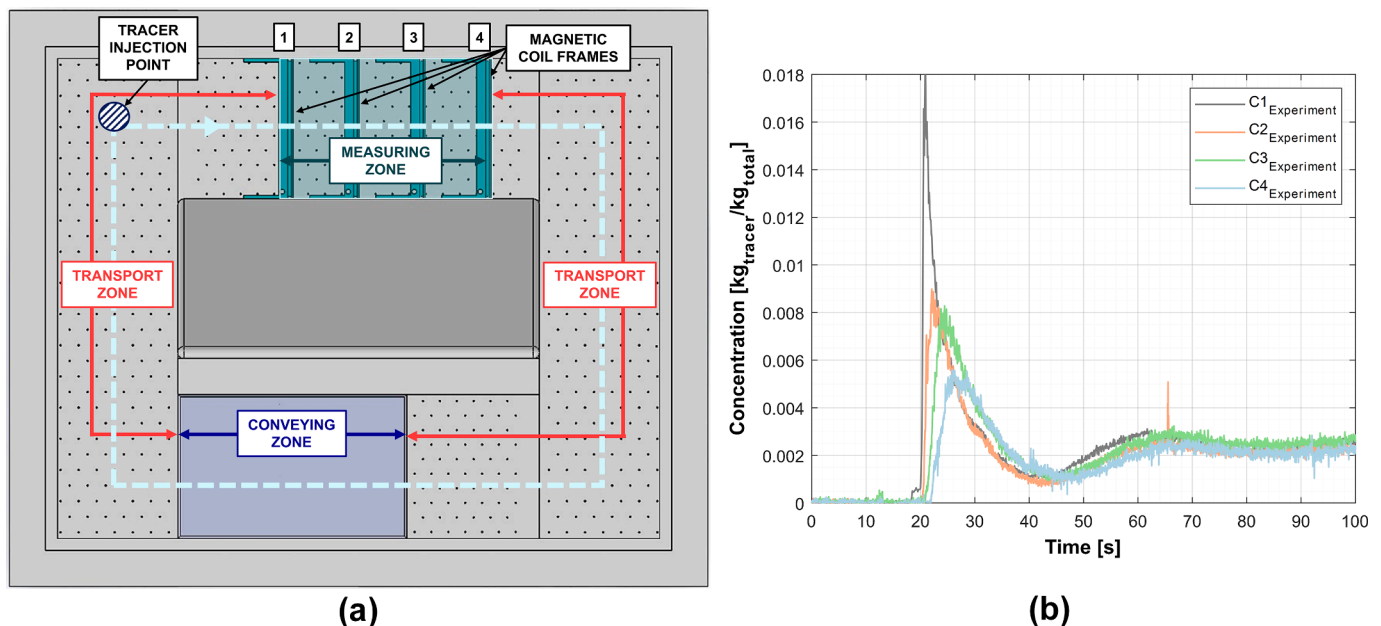


Fig. 3. Experimental setup used for the magnetic solids tracing method, together with the transient concentration profiles obtained. a) Top-view of the unit setting indicating the tracer injection point and the position of the four sensing coils. b) Example of transient profiles of the measured tracer concentration at different coils. Conditions: $FN_{TZ} = 3$, $H = 0.08$ m, $Q_{CZ} = 1.43 \times 10^{-2}$ m³/s.

using a customized cylindrical probe. Further description of the injection probe can be found in (Farha et al., 2024). The acquisition system measures, at a sampling frequency of 100 Hz, the impedance change caused by the tracer particles when transversing through the coils. The signal is converted to tracer concentration using a calibration curve previously obtained for each coil under various operational conditions (fluidization number and bed height), as detailed in Appendix A of (Farha et al., 2023). The calibration coefficient depends on the tracer material's properties—particularly its relative magnetic permeability—and the coil's sensitivity to tracer presence within the spatial region influenced by its magnetic field. Examples of the transient responses in each coil following tracer injection are given in Fig. 3b.

Table 2 provides a comparative analysis of the physical properties of both the bed and tracer materials, along with their dimensionless particle sizes ($Ar^{1/3}$). The experimental apparatus utilized in this study was constructed with a length scaling factor of 0.12. Further, the cold flow model is designed to simulate large-scale hot conditions, where silica sand, with an average particle size of 950 μm , is fluidized using flue gases at 800 °C.

Subsequent fitting of the data acquired from the MST experiments to the convection–dispersion transport equation Eq. (1) facilitates the determination the horizontal velocity, u_s , and dispersion coefficient, D_s , of the solids flow (details regarding the fitting procedure can be found in (Versteeg and Malalasekera, 2007):

$$\frac{\partial C}{\partial t} = \left(D_s \frac{\partial^2 C}{\partial x^2} \right) - u_s \frac{\partial C}{\partial x} \quad (1)$$

2.4. Assessment of solids convective transport

The energy flow provided by the conveying gas is expressed as:

$$E_{cz} = \frac{\gamma}{\gamma - 1} P_{\text{Atm}} Q_{cz} \left[\left(\frac{P_{\text{plenum}}}{P_{\text{Atm}}} \right)^{\frac{\gamma-1}{\gamma}} - 1 \right] \quad (2)$$

where P_{plenum} is the pressure within the gas plenum and Q_{cz} is the volumetric air flow injected into the conveying zone. The pressure was recorded for every volumetric flowrate of the fluidization agent inputted to the conveying zone. Data was acquired for 3 min and time-averaged.

The energy flow carried by the conveyed solids is calculated from the horizontal pressure drop experienced by the solids flow along the transport zone as:

$$E_s = u_s A_{Mz} \Delta P_{Tz} \quad (3)$$

The solids velocity is derived through the procedure outlined in Section 2.3., with A_{Mz} defining the cross-sectional area in the measurement zone. This is defined as the flow area perpendicular to the direction of the solids flow and is calculated as the product of the channel width and the expanded bed height under specific fluidization conditions. The net pressure drop across the transport zone, ΔP_{Tz} , is measured using pressure probes (Huba Control, piezoelectric type, precision > 0.5 % fs,

Table 2
Comparison of the materials used in the bed and magnetic tracer.

Parameter	Unit	Bed	Tracer
Material	–	Bronze	Iron-based alloy
Particle density (ρ_s)	kg/ m ³	8,770	7,988.3
Bulk density (ρ_b)	kg/ m ³	5,522.1	4,520
Particle size ($d_{10} - d_{50} - d_{90}$)	μm	80–112 – 132	25–69 – 123
Sauter mean particle size (d_{32})	μm	126	102
$Ar^{1/3}$	–	8.386	6.127
Minimum fluidization velocity (u_{mf})	m/s	0.074	0.039
Magnetic susceptibility	–	0	0.9

range ± 20 mbar) at a 5 Hz sampling rate. Pressure data are time-averaged over a 3-minute period for each experimental run, after verification of steady-state conditions.

The solids conveying efficiency attained during each experiment is calculated as the ratio of the energy flow imparted to the fluidized solids (associated with the net horizontal movement) to the energy inputted to the conveying configuration through gas injection:

$$\eta = \frac{E_s}{E_{cz}} \quad (4)$$

2.5. Kernel density estimation

The fluidized bed dynamics are quantified through pressure fluctuations, which indicate various operational states such as bubbling, slugging, turbulent, and dilute phase transport (Yates et al., 2016; Hartman and Trnka, 2008; Bai et al., 1996; van Ommen et al., 2011). The characteristics of these pressure fluctuations are analyzed using their probability density function (PDF) shape (Fan et al., 1981). A unimodal, symmetric PDF typically reflects stable bubbling behavior, where bubble formation, rise, and eruption occur in a relatively uniform and periodic manner (Bi et al., 2000; Fan et al., 1981; Xiang et al., 2018). This leads to consistent pressure fluctuations around the mean value. In contrast, bimodal or multi-modal PDFs suggest alternating or coexisting flow regimes, such as bubbling–slugging transitions or shifts between dense and dilute regions. These regimes exhibit irregular pressure fluctuations and more complex bed dynamics, as confirmed in earlier studies (Bi et al., 2000; Fan et al., 1981; Xiang et al., 2018). The width of the PDF reflects system variability. A broad PDF, with high variance in pressure fluctuations, indicates a chaotic state with significant kinetic energy transfer from gas to solids (van Ommen et al., 2011; Fan et al., 1981; Winter, 1968; Xiang et al., 2017). Conversely, a narrow PDF typically corresponds to more stable conditions, such as those observed in the slugging regime, where energy transfer is less erratic (Jaiboon et al., 2013; Chen et al., 2015). In this work, the pressure fluctuations in the plenum of the conveying zone are analyzed using the Kernel Density Estimation (KDE) method (see Appendix B for details on the equations applied). This is a non-parametric method that is ideally suited to estimating the probability density function (PDF) of continuous random variables, and it is especially advantageous when the distribution is unknown, as is the case in this study (Silverman, 2018).

2.6. Test matrix

Each of the five conveying mechanisms described in Section 2.2. was subjected to evaluation under different operational conditions, with variation of both the settled bed height (range of 0.08–0.10 m, corresponding to 0.67–0.83 m on upscaled basis) and the flowrate of conveying gas (in the range 0.001–0.125 m³/s, or 0.06–2.86 m³/s on upscaled basis). The upper limits are set to prevent the loss of bed material due to entrainment and to remain within the gas supply capacity of the laboratory. Conversely, the lower limits correspond to the minimum velocity required to maintain the functionality of the conveying mechanisms tested. In total, the investigation encompassed 62 different combinations of the operational parameters, each performed three times to ensure the robustness of the results.

With this, the expected operational regime for each mechanism studied (except for the slugging-based one) can be predicted by plotting the operational conditions on the Grace's fluidization regime map (Bi and Grace, 1995; Grace, 1986; Geldart, 1973), as presented in Fig. 4. The axes on the flow regime map are dimensionless, with the x-axis signifying the dimensionless particle diameter (the solids utilized here yield $Ar = 8.386$, as detailed in Table 2) and the y-axis representing the dimensionless superficial gas velocity achieved in the conveying zone. Equations (5) and (6) present the mathematical formulations of these quantities (Kunii and Levenspiel, 1991; Grace, 1986):

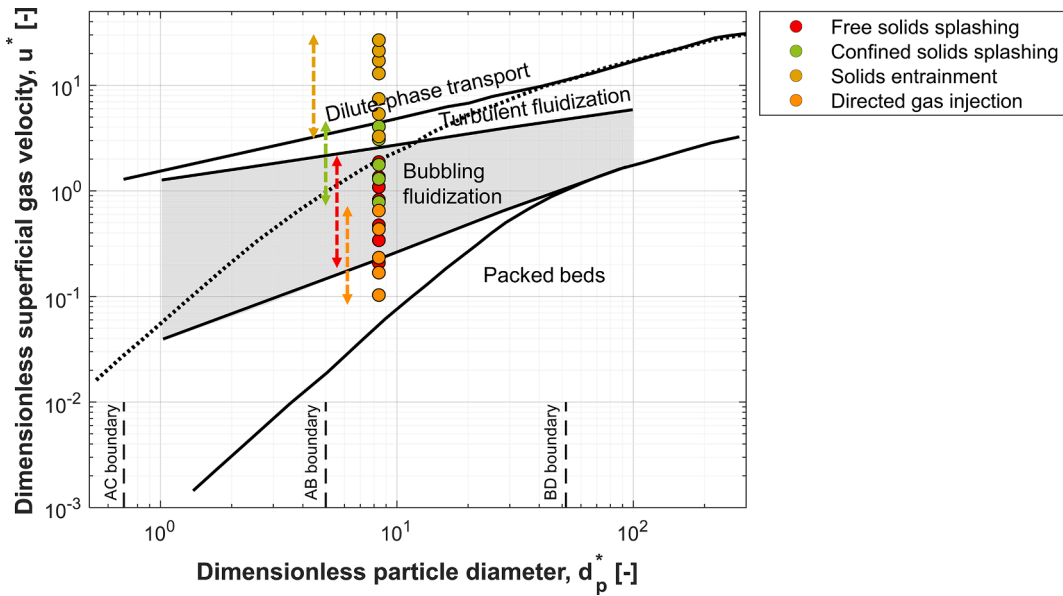


Fig. 4. Operational conditions for the different conveying mechanisms evaluated in this study, as displayed in Grace's fluidization regime map (Bi and Grace, 1995; Grace, 1986).

$$d_p^* = d_p \left[\frac{\rho_f(\rho_s - \rho_f)g}{\mu_f^2} \right]^{\frac{1}{3}} = Ar^{\frac{1}{3}} \quad (5)$$

$$u^* = u_0 \left[\frac{\rho_f^2}{\mu_f(\rho_s - \rho_f)g} \right]^{\frac{1}{3}} = \frac{Re_p}{Ar^{\frac{1}{3}}} \quad (6)$$

Regarding the solids conveying mechanism involving slugging, a different approach is used to tailor the design and operation to yield slugs. A crucial criterion for slugging to occur is that the height of the bed at the point of minimum fluidization must exceed a specific threshold, beyond which bubble coalescence leads to stable slug formation. According to Baeyens et al. (Baeyens and Geldart, 1974), this condition is expressed as:

$$H_{mf} > 1.3D_t^{0.75} \quad (7)$$

Furthermore, Stewart et al. (Stewart and Davidson, 1967) have formulated a criterion for the superficial gas velocity and defined the so-called minimum slugging velocity as:

$$u_{ms} = u_{mf} + 0.07(gD_t)^{0.5} \quad (8)$$

A critical assumption in this analysis is that the slug volume fraction is one-sixth of the total bed volume for a given cross-section (Bi and Grace, 1995; Stewart and Davidson, 1967). Furthermore, as the gas velocity is increased, a shift from slug-like formations to turbulent fluidization is observed. To ensure that the operations remain within the slugging fluidization regime, this transition must be avoided, i.e., the gas velocity must be kept below the transition velocity, u_{mt} (Bi et al., 2000; Cai, 1989):

$$\frac{u_{mt}}{\sqrt{gd_p}} = \left[\left(\frac{0.211}{D_t^{0.27}} + \frac{0.00242}{D_t^{1.27}} \right)^{\frac{1}{0.27}} \left(\frac{\rho_s - \rho_f}{\rho_f} \right) \left(\frac{D_t}{d_p} \right) \right]^{0.27} \quad (9)$$

For the solids and bed geometry utilized in this study, the minimum slugging fluidization velocity and the transition velocity were calculated to be 0.096 m/s and 1.974 m/s, respectively. Accordingly, the fluidization velocities employed in the slugging configuration ranged from 0.108 m/s to 1.769 m/s. In addition, visual observations were conducted during operation to verify the attainment of the intended

slugging regime.

Note that, as depicted in Fig. 2, both the slugging and solids entrainment configurations utilize a tubular module design, with the primary difference being the height of the module. Specifically, the module used for solids entrainment is twice as tall as that used for slugging. The slugging configuration is subject to a height limitation; beyond a certain module height, slug formation becomes unsustainable, either collapsing due to insufficient energy for upward movement or disintegrating into the turbulent regime at higher gas velocities.

3. Results and discussion

3.1. Pressure fluctuations analysis

Fig. 5 presents the (vertical) gas pressure drop (measured in the gas plenum) characteristic across the five different solids conveying mechanisms tested. As expected, the pressure drops follow a monotonously

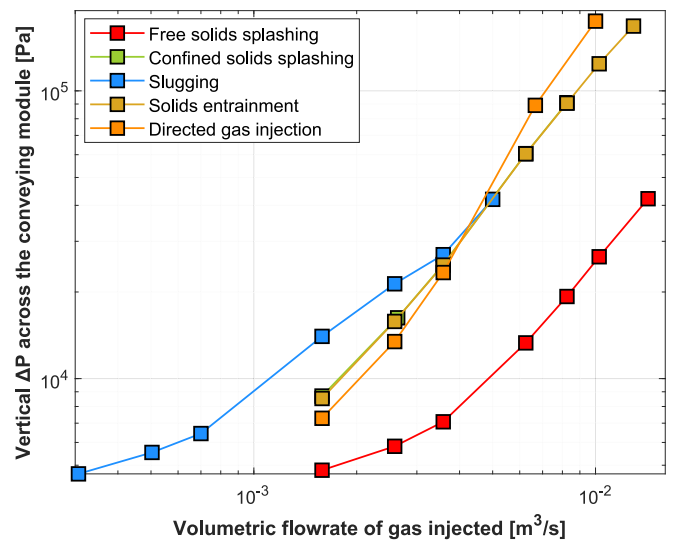


Fig. 5. Pressure drop in the gas plenum with respect to the injected gas flowrate for the solids conveying mechanisms studied. The presented values are downscaled.

increasing function with the volumetric flowrate of the conveying gas injected. Notably, the free solids splashing configuration exhibits the lowest pressure drop at any specified flowrate. Conversely, the slugging configuration is unique in its ability to operate at lower flowrates that are not attainable by the other configurations, although it exhibits a higher pressure drop at higher flowrates. This configuration also features a flatter pressure drop curve. The directed gas injection configuration displays a steep pressure drop curve, indicating that increased flowrates substantially increase energy costs. It must be noted that the comparison made here is indicative, and different nozzle designs may result in varying relationships between volumetric gas flow rate and pressure drop. Lastly, the confined solids splashing and solids entrainment configurations exhibit similar pressure drop profiles due to their identical flow areas and number of gas injection nozzles.

Fig. 6 depicts the probability density function (PDF) curves for pressure fluctuations across the different solids conveying mechanisms, for a selected bed height and flowrate of injected gas. Both the free solids splashing and slugging configurations exhibit unimodal distributions, meaning the pressure signal remains primarily close to its mean value rather than peaking at a non-zero value. This results in low variance, indicating consistent and predictable pressure fluctuations. This aligns with previous literature stating that bubbling fluidization at low gas velocity creates regular, small pressure fluctuations from bubble formation and bursting (Jaiboon et al., 2013; Falkowski and Brown, 2004; Bi, 2007; Johnsson et al., 2000), while slugging fluidization produces large, repetitive fluctuations due to the periodic rise of large gas slugs (Jaiboon et al., 2013; Chen et al., 2015). In contrast, confined solids splashing, solids entrainment, and directed gas injection configurations show bimodal distributions, reflecting the dominance of pressure values far from the mean and distinct fluctuations, and higher variance (Jaiboon et al., 2013; Falkowski and Brown, 2004; Bi, 2007; Johnsson et al., 2000). The data from the confined solids splashing configuration proves its design and operation aim to provide the largest pressure fluctuations, while the solids entrainment configuration also exhibits a pressure signal dominated by the fluctuating components. Although these fluctuations are of lower magnitude than those of confined solids splashing, they arise from the dynamic interplay between the gas flow and the solid particles being intermittently lifted and then settled (van Ommen et al., 2011; Jaiboon et al., 2013; Chen et al., 2015; Falkowski and Brown, 2004; Bi, 2007; Johnsson et al., 2000). Lastly, the PDF distribution for directed gas injection captures pressure fluctuations

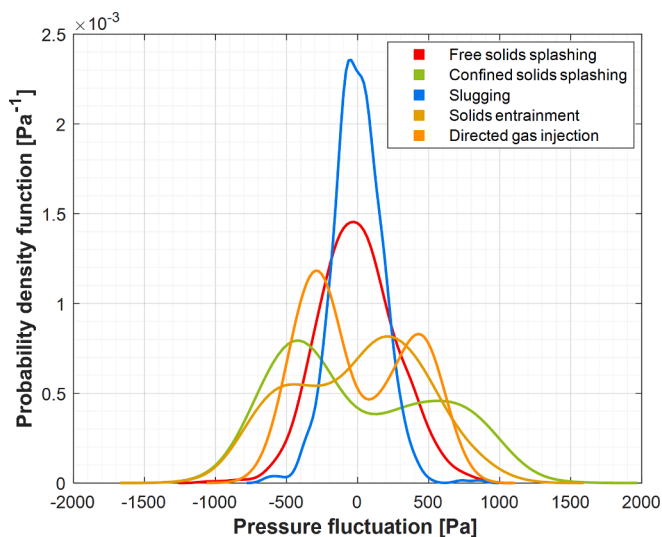


Fig. 6. Probability density functions of the pressure fluctuations across the five conveying mechanisms studied. Conditions used: $H = 0.08$ m, $Q_{CZ} = 1.58 \times 10^{-3}$ m³/s. The presented values are downscaled [Length scaling factor = 0.12].

caused by pulsating gas streams, resulting in alternating high-pressure zones during forceful injection and lower-pressure zones as the gas dissipates (Klinzing et al., 2010; Guo et al., 2001).

This analysis further explores the impacts of operational conditions on pressure fluctuations. Fig. 7 summarizes the results, displaying the standard deviations of the fluctuations across four operational conditions (characterized by (settled) bed height and volumetric flowrate in the conveying zone) for each solids conveying mechanism tested. In general, an increase in the gas flowrate injected into the conveying zone correlates with an increase in the variance of the pressure fluctuations. This is due to the higher kinetic energy imparted to the system, which enhances turbulence and intensifies the interactions between gas and solid particles, leading to greater variability in pressure changes (Falkowski and Brown, 2004; Bi, 2007; Johnsson et al., 2000). However, with the slugging configuration, an increase in bed height has the opposite effect. This suggests that while slugs continue to form and ascend, the higher bed height results in more-stable slug dynamics, thereby attenuating the intensity of the pressure fluctuations typically associated with their movement (Falkowski and Brown, 2004).

3.2. Solids conveying efficiency

Fig. 8 shows the correlation between the horizontal solids velocity (which is indicative of the forced solids circulation rate) and the volumetric flowrate of conveying gas, for the five different mechanisms tested. The highest solids velocity, 0.06 m/s (0.18 m/s in upscaled conditions) is attained in the free solids splashing configuration operated at the maximum gas flowrate (0.014 m³/s). The directed gas injection configuration also attained a notable solids circulation, with a solids velocity of 0.03 m/s (upscaled to 0.09 m/s) when operated at its maximum gas flow rate of 0.01 m³/s. The remaining mechanisms generally exhibit lower solids convective transport rate, up to 0.01 m/s (upscaled to 0.03 m/s). Furthermore, an increase in settled bed height causes an increase in solids velocities in all five mechanisms, particularly for the free solids splashing configuration. This is because, in the bubbling regime, a taller bed height allows bubbles to grow larger, leading to increased solids displacement induced by the bubble flow (Grace et al., 2020; Kunii and Levenspiel, 1991; Davidson et al., 1985; Leva, 1959).

To evaluate the operational characteristics of the tested solids conveying mechanisms, three key parameters were considered: flexibility, controllability, and data reliability. Flexibility—defined as the ability to generate a range of solids circulation rates from a single configuration—was quantified based on the circulation rates achieved across the tested gas flow rates. Controllability, defined as the ability to achieve a specific solids circulation rate by adjusting the air injection flow, was assessed using the normalized maximum slope of the \dot{m}_s-Q_{CZ} curve. This was calculated as the ratio of the maximum local slope to the mean slope across all available data points; higher values indicate that the solids response is concentrated within a narrow flow range, reflecting less uniform sensitivity to gas flow changes and, consequently, reduced controllability. Reliability reflects the consistency and reproducibility of the experimental results, quantified by the coefficient of variation of the solids circulation rate. This metric indicates the configuration's ability to maintain stable control over the solids flow rate. Table 3 summarizes these findings through a ranking system for each parameter, while Appendix C provides more detailed information on the analysis of these operational metrics.

Among the tested mechanisms, free solids splashing exhibited the most favorable overall performance. Directed gas injection also performed strongly, with high flexibility and controllability, though reliability was moderate. Solids entrainment showed a balanced profile, with moderate flexibility and controllability, and high reliability. In contrast, slugging and confined solids splashing both demonstrated low performance across most or all metrics, indicating limited operational range, poor responsiveness, and low measurement consistency.

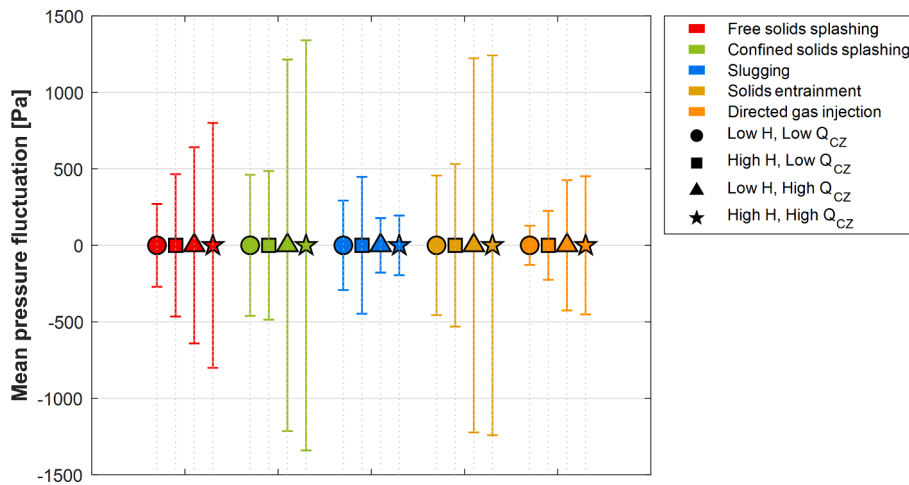


Fig. 7. Standard deviations of the pressure fluctuations across the tested solids conveying mechanisms, for different operational conditions.

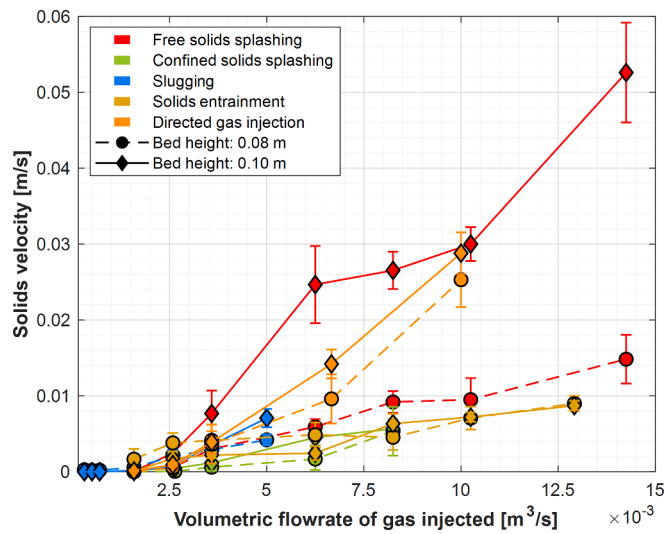


Fig. 8. Evaluation of conveyed solids velocity against gas volumetric flowrate for the solids conveying mechanisms tested. The presented values are down-scaled [Length scaling factor = 0.12].

To enable a comparison in terms of energy efficiency Eq. (4), beyond the attained solids flow, this study evaluates the capabilities of the different mechanisms to transfer energy from the injected gas to an effective macroscopic convective transport of solids. Fig. 9 plots the energy flow, represented by the conveyed flow of solids Eq. (3), as a function of the energy supplied by the gas injected into the conveying zone Eq. (2). Note that the values are in logarithmic scale, and there are

larger observed differences between some of the mechanisms. The free solids splashing configuration exhibits the highest energy transfer to solids convective transport for a given energy flow input within most of the studied range (5–1000 J/s). The slugging and directed gas injection configurations display similar intermediate results, with slugging outperforming the others for energy inputs below 10 J/s. The solids entrainment configuration performs the poorest at high energy flow inputs (>1000 J/s) but shows intermediate performance otherwise. Notably, the confined solids splashing configuration is the least effective at converting energy into effective horizontal convective transport of solids.

The free solids splashing configuration, operating under the bubbling regime, shows the highest efficiency for energy transfer. This suggests that the intense and localized interactions between rising gas bubbles and bed solids, which result in vigorous splashing, are particularly effective at converting gas energy into effective transport of solids at both meso- and macroscales (Hartman and Trnka, 2008; Bai et al., 1996; van Ommen et al., 2011; Jaiboon et al., 2013; Falkowski and Brown, 2004; Bi, 2007; Johnsson et al., 2000). In contrast, the confined solids splashing and solids entrainment configurations, which rely on more chaotic particle movement and high-velocity gas streams, respectively, demonstrate lower energy transfer efficiencies. This could be due to less-effective energy utilization seen under these turbulent conditions, where energy is dissipated in maintaining fluidization and mixing at smaller length scales rather than being effectively transferred to the solids in the wake of the well-defined bubbles characterizing the flow in the free solids splashing configuration (van Ommen et al., 2011; Jaiboon et al., 2013; Chen et al., 2015; Falkowski and Brown, 2004; Bi, 2007; Johnsson et al., 2000). Lastly, both the slugging and directed gas injection configurations deliver intermediate performance levels—possibly enhanced by substantial yet less chaotic solid–gas interactions—compared to the

Table 3
Comparative performance ranking of the tested solids conveying mechanisms.

Configurations	Flexibility	Controllability	Reliability
Free solids splashing	██████████	██████████	██████████
Confined solids splashing	██████	██████████	██████
Slugging	██████████	██████	██████████
Solids entrainment	██████████	██████████	██████████
Directed gas injection	██████████	██████████	██████████

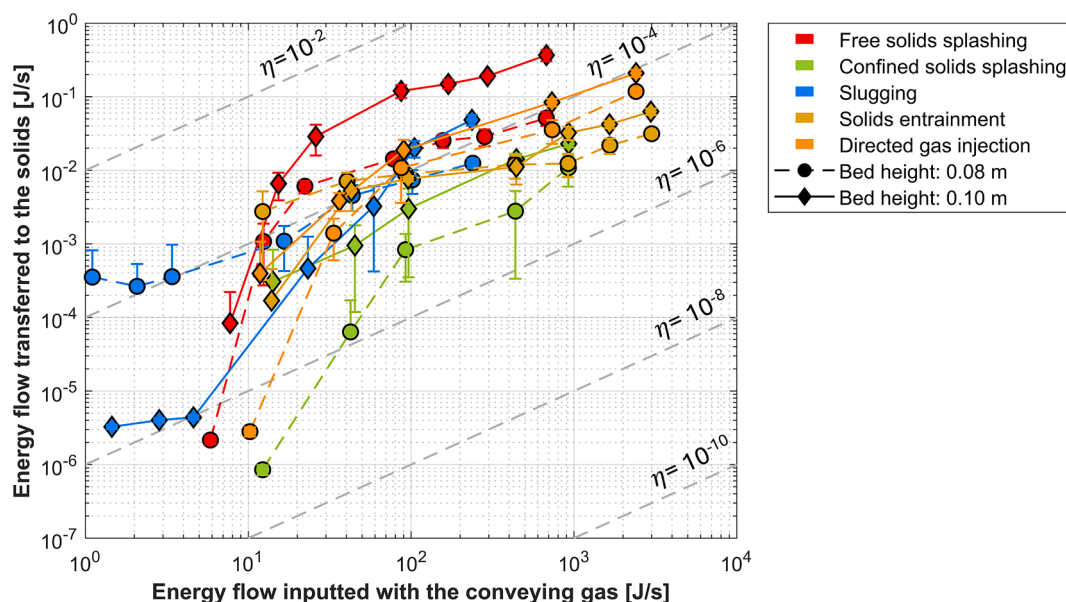


Fig. 9. Analysis of energy input versus solids energy flux for the tested solids conveying mechanisms in the present study. The dashed lines indicate the solids conveying efficiency (η). The presented values are downscaled [Length scaling factor = 0.12].

more turbulent conditions of the other configurations (Jaiboon et al., 2013; Chen et al., 2015; Guo et al., 2001). Thus, it is observed that regimes producing a clear differentiation in gas flow (i.e., well-defined bubbles or slugs) favor higher energy transfer to the intended macroscopic convective transport of solids. Additionally, higher beds generally enhance energy transfer efficiency, with this trend being most pronounced in the free solids splashing configuration.

To contextualize the solids circulation capabilities of the tested mechanisms, Fig. 10 compares the circulation rates achieved in this study (using upscaled values at 800 °C) with those reported for large-scale risers of Geldart B-type solids, namely circulating fluidized bed (CFB) furnaces (Mirek, 2016; Johnsson et al., 1995; Zhang et al., 1995;

Werdermann et al., 1992; Couturier et al., 1991; Johansson, 2005; Yang et al., 2005) and risers in dual fluidized bed (DFB) systems (Kaiser et al., 2003). The solids circulation flux is defined as the solids mass flow rate ' \dot{m}_s ' (see Appendix C) per unit cross-sectional area available for solids flow in the conveying zone (A_{cz}). In addition, the figure includes a dashed curve illustrating the experimentally derived expression by Djerf et al. Eq. (8) in (Djerf et al., 2022) for large-scale CFB furnaces. This curve depicts solids entrainment immediately above the splash zone as a function of fluidization velocity, i.e., showing how much Geldart-B solids a gas flow can entrain from the dense region in hot large-scale units before backmixing to the riser or furnace walls occurs.

Note that the comparison presented in Fig. 10 is not straightforward,

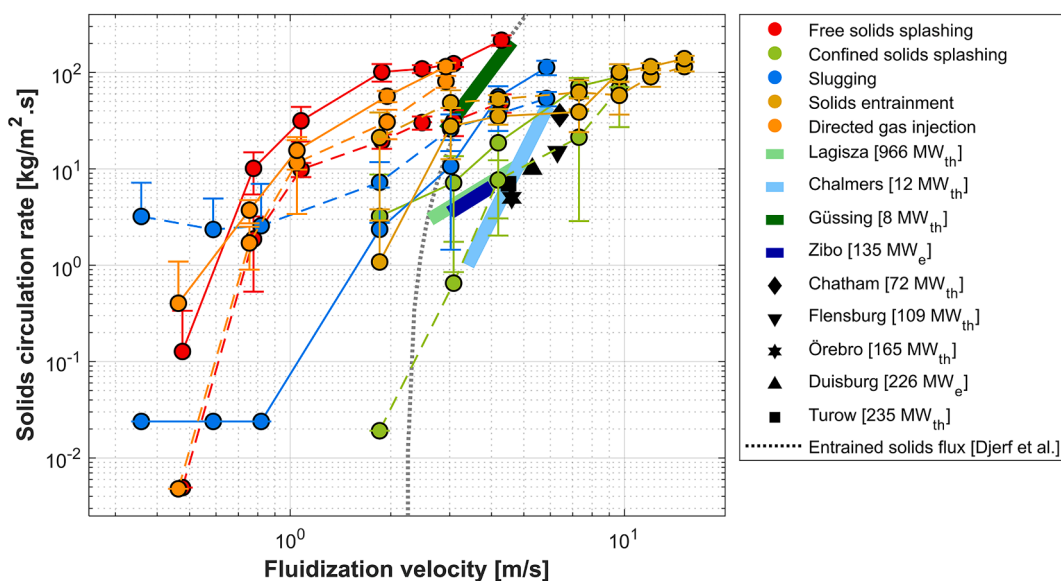


Fig. 10. Comparison of the solids circulation rates as a function of fluidization velocity from the current study (up-scaled) and large-scale risers operating with Geldart B-type solids in the literature (Mirek, 2016; Johnsson et al., 1995; Zhang et al., 1995; Werdermann et al., 1992; Couturier et al., 1991; Johansson, 2005; Yang et al., 2005; Kaiser et al., 2003; Djerf et al., 2022).

as CFB furnaces are not primarily designed to maximize solids external circulation, but rather to ensure adequate residence time and sufficient heat exchange surface area along the furnace walls. This results in tall and wide riser designs, with typical elutriated solids rates ranging within 1–50 kg/m²s. Furthermore, the CFB boiler data is derived from units with significant variations in size, and the solids circulation rates were inferred from a limited number of pressure measurements along the furnace height, without accounting for the backflow effect at the exit. This omission has been shown to potentially lead to significant overestimations of the net (i.e., external) solids circulation rate (Djerf et al., 2021; Wu et al., 2023). Despite these limitations, such data represents some of the few large-scale references available for external circulation involving Geldart B-type particles and are included here solely to provide contextual perspective.

Data in Fig. 10 indicate that large-scale CFB risers yield lower solids circulation rates than all the solids conveying mechanisms tested in this work, i.e., the alternative conveying configurations presented here can potentially provide solids circulation with reduced gas compression requirements. Particular note should be made of the data from the Güssing [8 MW_{th}] DFB (Kaiser et al., 2003), where the CFB riser was specifically designed to maximize solids circulation while ensuring sufficient residence time for combustion in a DFB system for indirect gasification. This is evidenced by its strong alignment with the empirical correlation curve from Djerf et al. (Djerf et al., 2022). Thus, this should serve as a relevant reference for the convective transport of Geldart B-type solids on an industrial scale. Compared to this industrial set-up (Kaiser et al., 2003), both the free solids splashing configuration (operating within the bubbling fluidization regime) and the directed gas injection exhibit a significantly higher performance in terms of solids conveying efficiency, with up-scaled solids circulation rates ranging within 5×10^{-2} – 2×10^3 kg/m² · s for fluidization velocities of 0.3–4.3 m/s.

4. Conclusions

This study investigates various methods to induce horizontal flow of fluidized Geldart B-type solids under bubbling conditions, with the aim of assessing various solids conveying mechanisms based on their efficiency, controllability, and flexibility. The experiments utilized a closed horizontal loop system, operated based on fluid-dynamical scaling principles, where magnetic tracing of solids was employed to assess the solids circulation rate. Five solids conveying configurations were evaluated: free solids splashing, confined solids splashing, slugging, solids entrainment, and directed gas injection. The experimental matrix for each mechanism included variations in the bed height and the injected gas flowrate to the conveying zone. First, pressure fluctuations in the plenum of the conveying configurations were analyzed to characterize the flow dynamics. Second, the solids conveying efficiency was assessed by relating the convective transport of solids attained to the energy loss of the conveying gas flow in the form of pressure drop.

Results indicate that both the confined solids splashing and solids entrainment configurations exhibit the highest pressure variances, suggesting strong solids agitation and efficient energy transfer from gas to

solids. However, these configurations exhibit the lowest performance in effectively transferring energy to macroscopic convective transport of solids in the horizontal direction, as the energy is primarily expended on turbulent mixing rather than being effectively used for macroscopic convective transport. Contrastingly, configurations based on regimes with well-defined gas structures (bubbles and slugs) emerge as the most effective at converting the energy input from the conveying gas into solids circulation. This is attributable to the lifting and displacement of particles induced during operation within the bubbling/slugging fluidization regime.

Subsequently, a comparison with literature results reveals that both the free solids splashing and directed gas injection configurations exceed previously reported solids circulation rates in large-scale CFB risers operating with Geldart B-type solids, including those specifically designed to promote solids circulation. These configurations achieve up-scaled rates in the range of 5×10^{-2} – 2×10^3 kg/m² · s at fluidization velocities between 1.9–4.3 m/s. Compared to conventional riser systems, some of the tested configurations offer improved energy efficiency and design compactness, achieving higher solids fluxes at lower gas flow rates. Notably, while several mechanisms performed well in terms of controllability and flexibility, only free solids splashing consistently combined these with high data reliability. In contrast, slugging and confined solids splashing showed low performance across most metrics, limiting their suitability for steady horizontal conveying.

Furthermore, it should be noted that the conclusions drawn in this study are specific to Geldart B-type particles, and their applicability to other particle classes requires further experimental validation.

CRedit authorship contribution statement

Munavara Farha: Writing – original draft, Validation, Methodology, Investigation, Formal analysis, Data curation. **Diana Carolina Guío-Pérez:** Writing – review & editing, Supervision, Conceptualization. **Filip Johnsson:** Writing – review & editing. **David Pallarès:** Writing – review & editing, Supervision, Funding acquisition, Conceptualization.

Declaration of competing interest

The authors declare the following financial interests/personal relationships which may be considered as potential competing interests: David Pallarès reports financial support was provided by Swedish Energy Agency. If there are other authors, they declare that they have no known competing financial interests or personal relationships that could have appeared to influence the work reported in this paper.

Acknowledgments

The authors acknowledge financial support from the Swedish Energy Agency within the framework of project 51182-1 – *Thermochemical poly-generation in heat and power plants*. The contribution of RISE Sensor Systems, which made possible the development of the Magnetic Solids Tracing system used in this work, is also acknowledged.

Appendix

Appendix A

Figure A.1 illustrates the configuration of the cold-flow experimental unit, featuring a transport zone and a conveying zone arranged around a central box in a closed-loop layout. The conveying zone incorporates five interchangeable configurations (Figure A.2) to drive horizontal solids crossflow. Airflow to the two zones is independently regulated through a hybrid system of rotameters and mass flow controllers. Bubbling condition in the transport zone is maintained at a fluidization number (u_0/u_{mf}) of 3, while the conveying zone operates under varying fluidization regimes (see Section 2.6). Flowrates required for both zones are calculated from their cross-sectional areas and supplied via dedicated air plenums. The induced solids circulation flux is computed using the horizontal solids velocity (u_s) obtained via magnetic solids tracing (MST) technique, as described in Section 2.3.

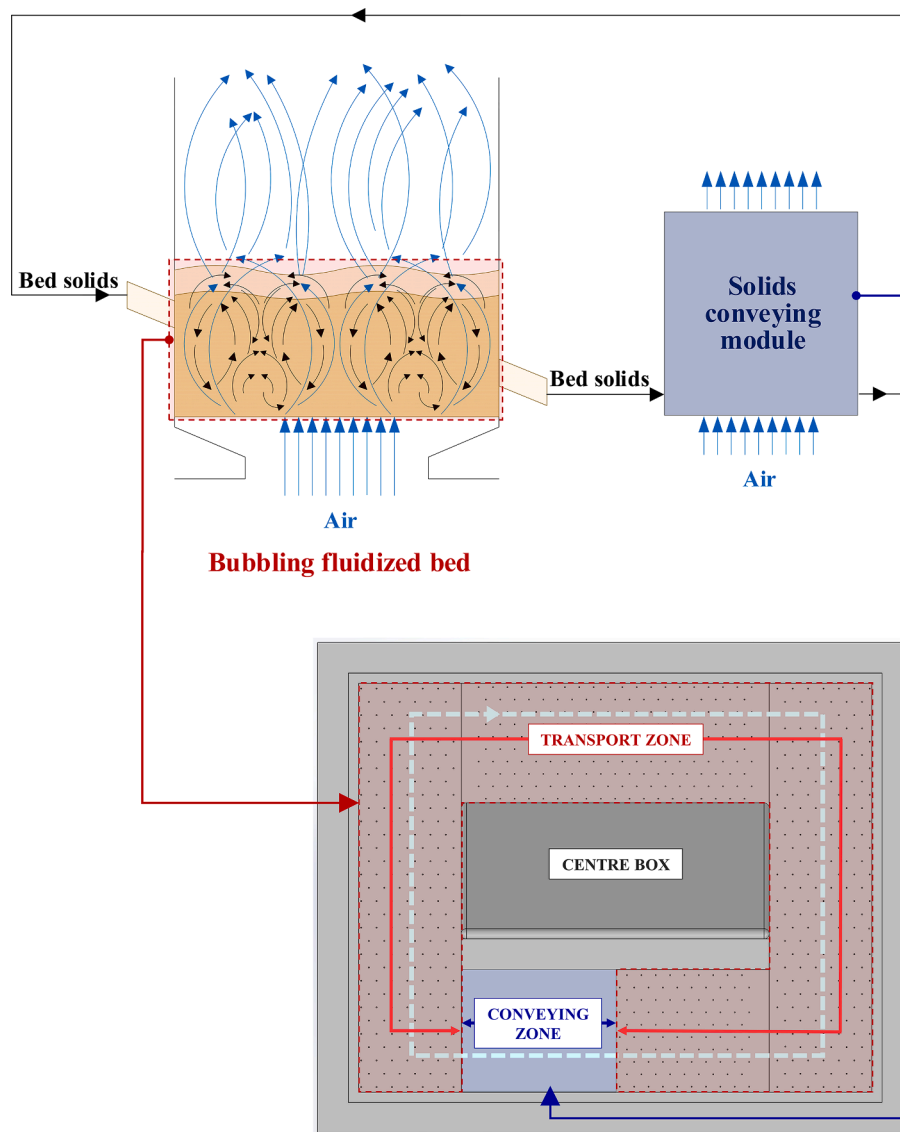


Figure A1. Schematic and top view of the cold-flow experimental unit, highlighting the correspondence between system components and their physical layout.

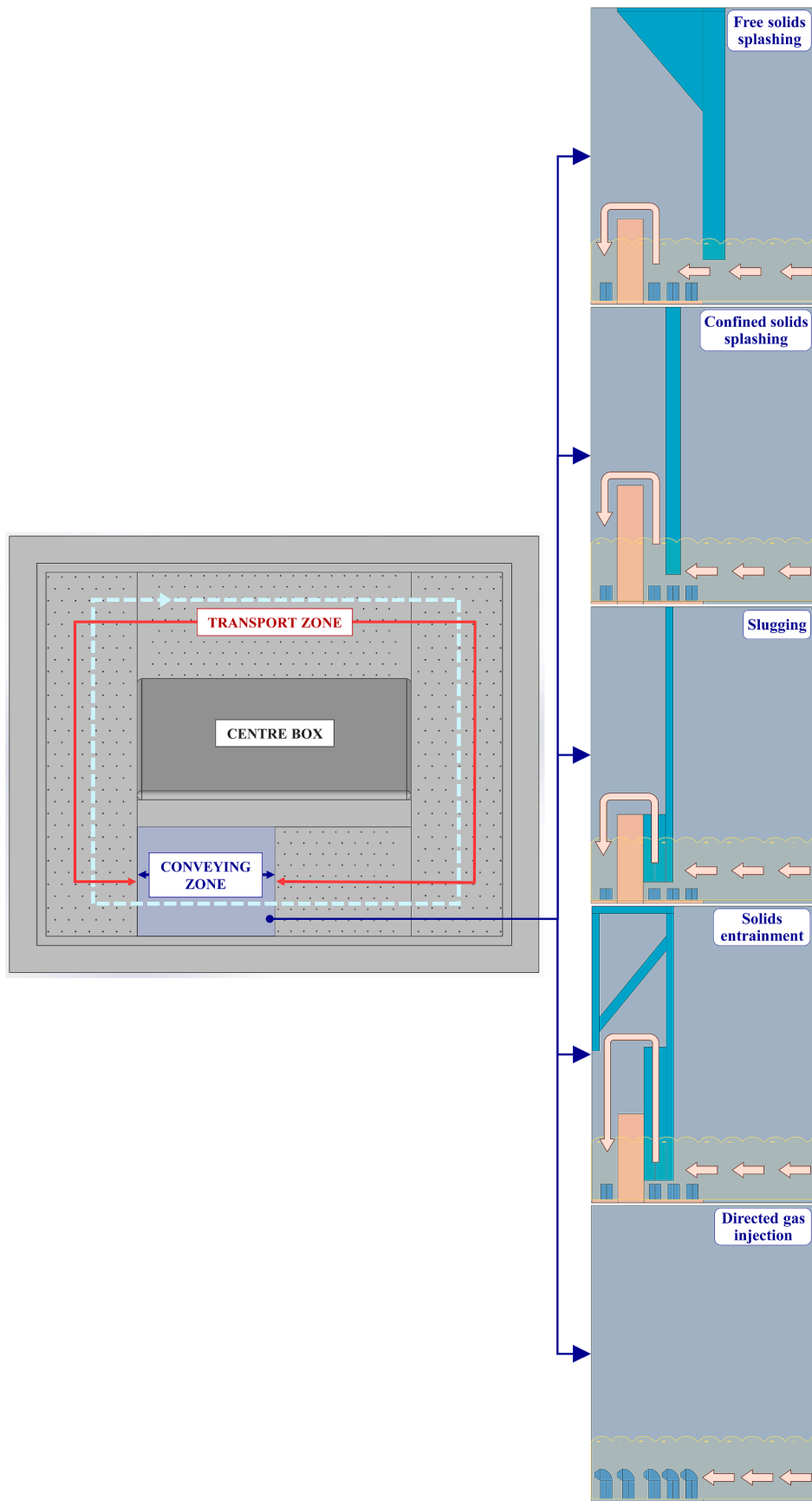


Figure A2. Five configurations demonstrating different ways the solids conveying zone can be modified, with flow direction and operating principles illustrated.

Appendix B

KDE (kernel density estimation) is a non-parametric method to estimate the probability density function of a continuous random variable (Silverman, 2018). It is particularly useful for data analysis where the underlying distribution is unknown. KDE is implemented using a kernel function that smooths out the data points across the range, providing a continuous and smooth estimation of the probability density (Silverman, 2018). The estimated probability density function for a set of pressure fluctuations, denoted as $\hat{f}(P')$, can be expressed as shown in the equation below (Silverman, 2018):

$$\hat{f}(P') = \frac{1}{nh} \sum_{i=1}^n K\left(\frac{P' - P_i}{h}\right) \quad (\text{A.1})$$

where 'n' denotes the number of data points.

The bandwidth 'h' in KDE is crucial, and selecting an appropriate value is essential to avoid overfitting or excessive smoothing. This can be achieved using Silverman's rule of thumb (Silverman, 2018).

$$h = 1.06 \cdot \sigma \cdot n^{-1/5} \quad (\text{A.2})$$

where 'σ' is the standard deviation of the data.

K represents the kernel function, typically a Gaussian (bell-shaped) curve, which is used to weigh the data points around P' (Silverman, 2018):

$$K = \frac{1}{\sqrt{2\pi}} e^{-\frac{\left(\frac{P' - P_i}{h}\right)^2}{2}} \quad (\text{A.3})$$

Figure A.3 depicts the probability density function (PDF) plots for the pressure fluctuations observed across five distinct conveying mechanisms characterized by unique flow properties: free solids splashing, confined solids splashing, slugging, solids entrainment, and directed gas injection. This statistical method enables the identification of predominant pressure behaviors for each configuration, providing a robust basis for evaluating system performance. The analysis further explores the impacts of operational conditions on pressure dynamics, focusing on four operational scenarios, as determined by specific combinations of fixed bed heights and volumetric flowrates of the injected air.

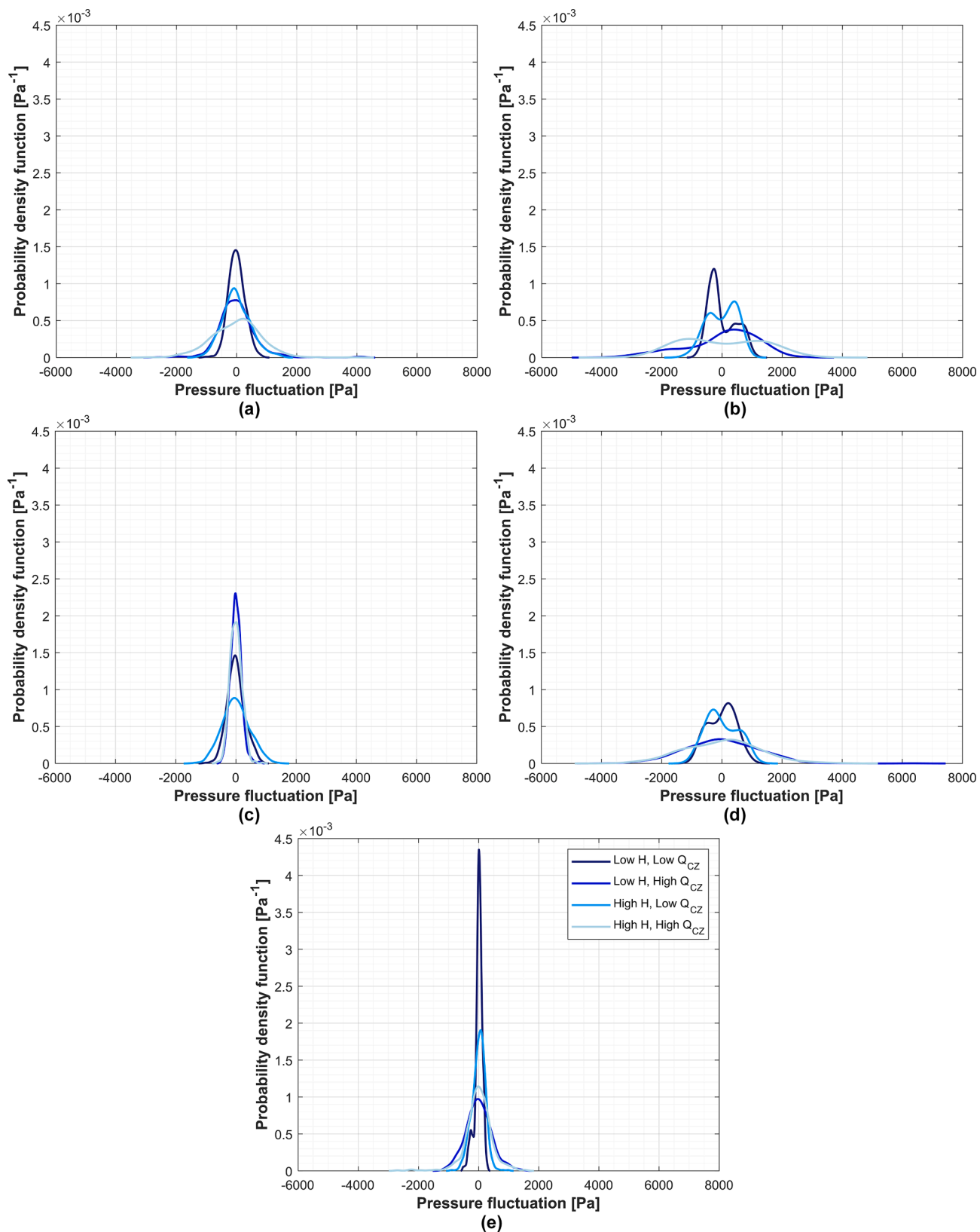


Figure A3. Probability density function (PDF) plots of pressure fluctuations for the solids conveying mechanisms under various operational conditions: (a) Free solids splashing, (b) Confined solids splashing, (c) Slugging, (d) Solids entrainment, and (e) Directed gas injection.

Appendix C

Three performance metrics were used to evaluate the operational characteristics of each solids conveying mechanism: flexibility, controllability, and reliability. These were derived from the relationship between the solids circulation rate ' \dot{m}_s ' and the gas volumetric flowrate in the conveying zone ' Q_{cz} '. The solids circulation rate was computed as:

$$\dot{m}_s = u_s \rho_s \varepsilon_s A_{mz} \quad (\text{A.4})$$

Note that this calculation directly scales solids velocity by system parameters, so the resulting trends mirror those in Fig. 8; thus, no additional figure is included.

Flexibility was defined as the range of \dot{m}_s values observed across the tested Q_{cz} , representing the operational breadth of each mechanism:

$$R = \max(\dot{m}_s) - \min(\dot{m}_s) \quad (\text{A.5})$$

Controllability was evaluated using the local slope of the \dot{m}_s - Q_{cz} relationship. A normalized controllability index was computed as:

$$CI_{\dot{m}_s} = \frac{\max\left[\frac{\Delta\dot{m}_s}{\Delta Q_{cz}}\right]}{\text{mean}\left[\frac{\Delta\dot{m}_s}{\Delta Q_{cz}}\right]} \quad (\text{A.6})$$

Data reliability was assessed by calculating the coefficient of variation of the solids circulation rate:

$$CV_{\dot{m}_s} = \frac{\sigma_{\dot{m}_s}}{\bar{\dot{m}_s}} \quad (\text{A.7})$$

Table A1 summarizes the evaluated performance metrics, derived from the \dot{m}_s - Q_{cz} relationship, across all tested conveying configurations.

Table A1

Summary of operational performance metrics for the tested conveying configurations.

Operation metrics		Flexibility		Controllability		Reliability
Configurations	H[m]	\dot{m}_s [kg/s]	R [kg/s]	Slope [kg/m ³]	$CI_{\dot{m}_s}$ [-]	$CV_{\dot{m}_s}$ [-]
Free solids splashing	0.08	$5.4 \times 10^{-5} - 5.4 \times 10^{-1}$	5.4×10^{-1}	43.5 ± 29.1	2.02	0.29 ± 0.22
	0.10	$1.4 \times 10^{-3} - 2.4 \times 10^0$	2.4×10^0	168.3 ± 103.8	1.71	0.43 ± 0.56
Confined solids splashing	0.08	$5.4 \times 10^{-5} - 1.9 \times 10^{-1}$	1.9×10^{-1}	25.9 ± 28.1	2.56	0.94 ± 0.51
	0.10	$9.1 \times 10^{-3} - 2.6 \times 10^{-1}$	2.5×10^{-1}	32.0 ± 19.1	1.77	0.79 ± 0.62
Slugging	0.08	$6.7 \times 10^{-3} - 1.5 \times 10^{-1}$	1.5×10^{-1}	20.6 ± 23.5	2.58	0.80 ± 0.57
	0.10	$6.8 \times 10^{-5} - 3.2 \times 10^{-1}$	3.2×10^{-1}	45.5 ± 59.3	2.82	0.76 ± 0.71
Solids entrainment	0.08	$6.0 \times 10^{-2} - 3.3 \times 10^{-1}$	2.7×10^{-1}	27.6 ± 30.1	2.81	0.33 ± 0.24
	0.10	$3.1 \times 10^{-3} - 3.9 \times 10^{-1}$	3.9×10^{-1}	38.9 ± 34.2	2.26	0.45 ± 0.57
Directed gas injection	0.08	$5.4 \times 10^{-5} - 9.2 \times 10^{-1}$	9.2×10^{-1}	92.9 ± 64.1	1.83	0.41 ± 0.24
	0.10	$4.6 \times 10^{-3} - 1.3 \times 10^0$	1.3×10^0	130.2 ± 67.4	1.52	0.52 ± 0.67

Data availability

Data will be made available on request.

References

- Adánéz, J., Gayán, P., Celaya, J., De Diego, L.F., García-Labiano, F., Abad, A., 2006. Chemical looping combustion in a 10 kWth prototype using a CuO/Al₂O₃ oxygen carrier: effect of operating conditions on methane combustion. *Ind. Eng. Chem. Res.* 45, 6075–6080. <https://doi.org/10.1021/ie060364l>.
- Baeyens, J., Geldart, D., 1974. An investigation into slugging fluidized beds. *Chem. Eng. Sci.* 29, 255–265. [https://doi.org/10.1016/0009-2509\(74\)85051-7](https://doi.org/10.1016/0009-2509(74)85051-7).
- Bai, D., Shibuya, E., Nakagawa, N., Kato, K., 1996. Characterization of gas fluidization regimes using pressure fluctuations. *Powder Technol.* 87, 105–111. [https://doi.org/10.1016/0032-5910\(95\)03072-7](https://doi.org/10.1016/0032-5910(95)03072-7).
- Bao, J., Li, Z., Sun, H., Cai, N., 2013. Continuous test of ilmenite-based oxygen carriers for chemical looping combustion in a dual fluidized bed reactor system. *Ind. Eng. Chem. Res.* 52, 14817–14827. <https://doi.org/10.1021/ie4025209>.
- Bi, H.T., 2007. A critical review of the complex pressure fluctuation phenomenon in gas–solids fluidized beds. *Chem. Eng. Sci.* 62, 3473–3493. <https://doi.org/10.1016/j.ces.2006.12.092>.
- Bi, H.T., Ellis, N., Abba, I.A., Grace, J.R., 2000. A state-of-the-art review of gas–solid turbulent fluidization. *Chem. Eng. Sci.* 55, 4789–4825. [https://doi.org/10.1016/S0009-2509\(00\)00107-X](https://doi.org/10.1016/S0009-2509(00)00107-X).
- Bi, H.T., Grace, J.R., 1995. Flow regime diagrams for gas–solid fluidization and upward transport. *Int. J. Multiph. Flow* 21, 1229–1236. [https://doi.org/10.1016/0301-9322\(95\)00037-X](https://doi.org/10.1016/0301-9322(95)00037-X).
- C.C. Werdermann, Ph.D. Dissertation, Technical University of Hamburg, Harburg., 1992.
- P. Cai, The transition of flow regime in dense phase gas–solid fluidized bed, 1989.
- Charitos, A., Hawthorne, C., Bidwe, A.R., Korovesis, L., Schuster, A., Scheffknecht, G., 2010. Hydrodynamic analysis of a 10kWth calcium looping dual fluidized bed for post-combustion CO₂ capture. *Powder Technol.* 200, 117–127. <https://doi.org/10.1016/j.powtec.2010.02.012>.
- Chen, Y., Jim Lim, C., Grace, J.R., Zhang, J., Zhao, Y., Zheng, C., 2015. Characterization of pressure fluctuations from a gas–solid fluidized bed by structure density function analysis. *Chem. Eng. Sci.* 129, 156–167. <https://doi.org/10.1016/j.ces.2015.02.009>.
- Couturier, M., Doucette, B., Stevens, D., Poolpol, S., Razbin, V., 1991. Temperature, gas concentration and solid mass flux profiles within a large circulating fluidized bed combustor. In: *Proceedings of the International Conference on Fluidized Bed Combustion*, pp. 107–114.
- J.F. Davidson, R. Clift, D. Harrison, *Fluidization*, 2. ed., Academic, 1985. <https://search.ebscohost.com/login.aspx?direct=true&db=cac09075a&AN=clpc.oai.edge.chalmers.folio.ebsco.com.fs00001000.1caecdbe.3593.4bd9.a758.6c5fb8dd8859&site=eds-live&scope=site&authtype=guest&custid=s3911979&groupid=main&profile=eds>.

- Dawe, M., Briens, C., Berruti, F., 2008. Study of horizontal sonic gas jets in gas-solid fluidized beds. *Can. J. Chem. Eng.* 86, 506–513. <https://doi.org/10.1002/cjce.20065>.
- Djerf, T., Pallarès, D., Johnsson, F., 2021. Solids flow patterns in large-scale circulating fluidised bed boilers: Experimental evaluation under fluid-dynamically down-scaled conditions. *Chem. Eng. Sci.* 231, 116309. <https://doi.org/10.1016/j.ces.2020.116309>.
- Djerf, T., Pallarès, D., Johnsson, F., 2022. Solids backmixing and entrainment in the splash zone of large-scale fluidized bed boilers. *Powder Technol.* 404. <https://doi.org/10.1016/j.powtec.2022.117471>.
- Falkowski, D., Brown, R.C., 2004. Analysis of pressure fluctuations in fluidized beds. *Ind. Eng. Chem. Res.* 43, 5721–5729. <https://doi.org/10.1021/ie030684u>.
- Fan, L.T., Ho, T.-C., Hiraoka, S., Walawender, W.P., 1981. Pressure fluctuations in a fluidized bed. *AIChE J* 27, 388–396. <https://doi.org/10.1002/aic.690270308>.
- Fan, L., Toda, M., 1983. Hold-up of fine Particles in the packed dense bed of the Multisolid pneumatic. *Transport Bed*.
- Fang, F., Li, Z.S., Cai, N.S., 2009. Continuous CO₂ capture from flue gases using a dual fluidized bed reactor with calcium-based sorbent. *Ind. Eng. Chem. Res.* 48, 11140–11147. <https://doi.org/10.1021/ie901128r>.
- Farha, M., Guío-Pérez, D.C., Aronsson, J., Johnsson, F., Pallarès, D., 2023. Assessment of experimental methods for measurements of the horizontal flow of fluidized solids under bubbling conditions. *Fuel* 348. <https://doi.org/10.1016/j.fuel.2023.128515>.
- Farha, M., Guío-Pérez, D.C., Johnsson, F., Pallarès, D., 2024. Characterization of the solids crossflow in a bubbling fluidized bed. *Powder Technol.*, 119967 <https://doi.org/10.1016/j.powtec.2024.119967>.
- Foscolo, P.U., Germanà, A., Jand, N., Rapagnà, S., 2007. Design and cold model testing of a biomass gasifier consisting of two interconnected fluidized beds. *Powder Technol.* 173, 179–188. <https://doi.org/10.1016/j.powtec.2007.01.008>.
- Geldart, D., 1973. Types of gas fluidization. *Powder Technol.* 7, 285–292. [https://doi.org/10.1016/0032-5910\(73\)80037-3](https://doi.org/10.1016/0032-5910(73)80037-3).
- Glicksman, L.R., 1988. Scaling relationships for fluidized beds. *Chem. Eng. Sci.* 43, 1419–1421. [https://doi.org/10.1016/0009-2509\(88\)85118-2](https://doi.org/10.1016/0009-2509(88)85118-2).
- L.R. Glicksman, M. Hyre, K. Woloshun, Simplified scaling relationships for fluidized beds, 1993.
- Grace, J.R., 1986. Contacting modes and behaviour classification of gas—solid and other two-phase suspensions. *Can. J. Chem. Eng.* 64, 353–363. <https://api.semanticscholar.org/CorpusID:96755090>.
- Grace, J., Bi, X., Ellis, N., 2020. Essentials of fluidization technology. Wiley. <https://doi.org/10.1002/9783527699483>.
- Guío-Pérez, D.C., Dietrich, F., Ferreira Cala, J.N., Pröll, T., Hofbauer, H., 2017. Estimation of solids circulation rate through magnetic tracer tests. *Powder Technol.* 316, 650–657. <https://doi.org/10.1016/j.powtec.2017.04.062>.
- Guo, Q., Yue, G., Liu, Z., 2001. Gas Discharge patterns in a Large jetting fluidized bed with a vertical nozzle. *Ind. Eng. Chem. Res.* 40, 3689–3696. <https://doi.org/10.1021/ie000912+>.
- Hartman, M., Trnka, O., 2008. Physical characteristics of fluidized beds via pressure fluctuation analysis. *AIChE J* 54, 1761–1769. <https://doi.org/10.1002/aic.11518>.
- Hawthorne, C., Poboss, N., Dieter, H., Gredinger, A., Zieba, M., Scheffknecht, G., 2012. Operation and results of a 200-kWth dual fluidized bed pilot plant gasifier with adsorption-enhanced reforming. *Biomass Convers. Biorefin.* 2, 217–227. <https://doi.org/10.1007/s13399-012-0053-3>.
- Hilgraf, P., 2024. Modern dense phase conveying methods. In: Hilgraf, P. (Ed.), *Pneumatic Conveying: Basics, Design and Operation of Plants*. Springer, Berlin Heidelberg, Berlin, Heidelberg, pp. 279–305. https://doi.org/10.1007/978-3-662-67223-5_6.
- Jaiboon, O., Chalermisinsuwan, B., Mekasut, L., Piumsomboon, P., 2013. Effect of flow pattern on power spectral density of pressure fluctuation in various fluidization regimes. *Powder Technol.* 233, 215–226. <https://doi.org/10.1016/j.powtec.2012.09.014>.
- A. Johnsson, Solids flow pattern in circulating fluidized-bed boilers., 2005.
- Johnsson, F., Zhang, W., Leckner, B., 1995. Characteristics of the formation of particle wall layers in CFB boilers. In: *Proceedings of the Second International Conference on Multiphase Flow*, pp. 25–32.
- Johnsson, F., Zijerveld, R.C., Schouten, J.C., van den Bleek, C.M., Leckner, B., 2000. Characterization of fluidization regimes by time-series analysis of pressure fluctuations. *Int. J. Multiph. Flow* 26, 663–715. [https://doi.org/10.1016/S0301-9322\(99\)00028-2](https://doi.org/10.1016/S0301-9322(99)00028-2).
- Kaewluan, S., Pipatmanomai, S., 2011. Gasification of high moisture rubber woodchip with rubber waste in a bubbling fluidized bed. *Fuel Process. Technol.* 92, 671–677. <https://doi.org/10.1016/j.fuproc.2010.11.026>.
- Kaisers, S., Löffler, G., Bosch, K., Hofbauer, H., 2003. Hydrodynamics of a dual fluidized bed gasifier Part II: simulation of solid circulation rate, pressure loop and stability. *Chem. Eng. Sci.* 58, 4215–4223. [https://doi.org/10.1016/S0009-2509\(03\)00233-1](https://doi.org/10.1016/S0009-2509(03)00233-1).
- G.E. Klinzing, F. Rizk, R. Marcus, L.S. Leung, Feeding of Pneumatic Conveying Systems, in: G.E. Klinzing, F. Rizk, R. Marcus, L.S. Leung (Eds.), *Pneumatic Conveying of Solids: A Theoretical and Practical Approach*, Springer Netherlands, Dordrecht, 2010: pp. 237–302. https://doi.org/10.1007/978-90-481-3609-4_7.
- D. Kumii, O. Levenspiel, Fluidization engineering., 2. ed., Butterworth-Heinemann, 1991. <https://search.ebscohost.com/login.aspx?direct=true&db=cac09075a&AN=clpc.oai.edge.chalmers.folio.ebsco.com.fs00001000.cfe5a823.1497.4690.b602>.
- bbd293482377&site=eds-live&scope=site&authtype=guest&custid=s3911979&groupid=main&profile=eds.
- Kuramoto, M., Kumii, D., Furusawa, T., 1986. Flow of dense fluidized Particles through an opening in a circulation. System.
- M. Leva, Fluidization., McGraw-Hill, 1959. <https://search.ebscohost.com/login.aspx?direct=true&db=cac09075a&AN=clpc.oai.edge.chalmers.folio.ebsco.com.fs00001000.8087a3c8.c70b.423f.954b.e7d58d878d8f&site=eds-live&scope=site&authtype=guest&custid=s3911979&groupid=main&profile=eds>.
- Li, Y.H., Chen, Z., Watkinson, P., Bi, X., Grace, J., Lim, C.J., Ellis, N., 2018. A novel dual-bed for steam gasification of biomass. *Biomass Convers. Biorefin.* 8, 357–367. <https://doi.org/10.1007/s13399-017-0288-0>.
- Linderholm, C., Abad, A., Mattisson, T., Lyngfelt, A., 2008. 160 h of chemical-looping combustion in a 10 kW reactor system with a NiO-based oxygen carrier. *Int. J. Greenhouse Gas Control* 2, 520–530. <https://doi.org/10.1016/j.ijggc.2008.02.006>.
- Luo, H., Lin, W., Song, W., Li, S., Dam-Johansen, K., Wu, H., 2019. Three dimensional full-loop CFD simulation of hydrodynamics in a pilot-scale dual fluidized bed system for biomass gasification. *Fuel Process. Technol.* 195. <https://doi.org/10.1016/j.fuproc.2019.106146>.
- Luo, Z., Lin, Y., Tu, Q., Yang, W., Wang, H., 2020. Investigation of gas–solids flow hydrodynamics in a cold model of a dual fluidised bed gasifier using electrical capacitance tomography sensors. *Particuology* 51, 193–204. <https://doi.org/10.1016/j.partic.2019.11.003>.
- Mirek, P., 2016. Influence of the model scale on hydrodynamic scaling in CFB boilers. *Braz. J. Chem. Eng.* 33.
- Nguyen, T.D.B., Seo, M.W., Il Lim, Y., Song, B.H., Kim, S.D., 2012. CFD simulation with experiments in a dual circulating fluidized bed gasifier. *Comput. Chem. Eng.* 36, 48–56. <https://doi.org/10.1016/j.compchemeng.2011.07.005>.
- A. Reichhold, H. Hofbauer, Internally circulating fluidized bed for continuous adsorption and desorption, 1995.
- Rubio, O., Herguido, J., Menéndez, M., Grasa, G., Abanades, J.C., 2004. Oxidative dehydrogenation of butane in an interconnected fluidized-bed reactor. *AIChE J* 50, 1510–1522. <https://doi.org/10.1002/aic.10134>.
- Santana, D., Nauri, S., Acosta, A., García, N., Macías-Machín, A., 2005. Initial particle velocity spatial distribution from 2-D erupting bubbles in fluidized beds. *Powder Technol.* 150, 1–8. <https://doi.org/10.1016/j.powtec.2004.11.013>.
- Silverman, B.W., 2018. *Density estimation for statistics and data analysis*. Routledge.
- O.C. Snip, M. Woods I, R. Korbee, J.C. Schouten, C.M. Van Den Bleek, Regenerative removal of SO₂ and NO_x for a 150 MWe power plant in an interconnected fluidized bed facility, 1996.
- Stewart, P.S.B., Davidson, J.F., 1967. Slug flow in fluidised beds. *Powder Technol.* 1, 61–80. [https://doi.org/10.1016/0032-5910\(67\)80014-7](https://doi.org/10.1016/0032-5910(67)80014-7).
- van Ommen, J.R., Sasic, S., van der Schaaf, J., Gheorghiu, S., Johnsson, F., Coppens, M.-O., 2011. Time-series analysis of pressure fluctuations in gas–solid fluidized beds – a review. *Int. J. Multiph. Flow* 37, 403–428. <https://doi.org/10.1016/j.ijmultiphaseflow.2010.12.007>.
- H.K. Versteeg W. Malalasekera An Introduction to Computational Fluid Dynamics: the Finite volume method 2nd ed, 2007 Pearson Education Ltd Harlow, England; New York.
- Werner, D., Windows-Yule, C.R.K., Kokalova-Wheldon, T., Seville, J.P.K., 2023. Influence of nozzle design on flow, mixing, and fluidisation in a bubbling bed fluidised by a single nozzle. *Mech. Res. Commun.* 132. <https://doi.org/10.1016/j.mechrescom.2023.104180>.
- Winter, O., 1968. Density and pressure fluctuations in gas fluidized beds. *AIChE J* 14, 426–434. <https://doi.org/10.1002/aic.690140317>.
- Wu, W., Leckner, B., Pallarès, D., Duan, L., 2023. Solids separation efficiency at the outlet of a circulating fluidized bed riser. *Powder Technol.* 428, 118748. <https://doi.org/10.1016/j.powtec.2023.118748>.
- Xiang, J., Li, Q., Tan, Z., Zhang, Y., 2017. Characterization of the flow in a gas–solid bubbling fluidized bed by pressure fluctuation. *Chem. Eng. Sci.* 174, 93–103. <https://doi.org/10.1016/j.ces.2017.09.001>.
- Xiang, J., Li, Q., Wang, A., Zhang, Y., 2018. Mathematical analysis of characteristic pressure fluctuations in a bubbling fluidized bed. *Powder Technol.* 333, 167–179. <https://doi.org/10.1016/j.powtec.2018.04.030>.
- Xu, G., Murakami, T., Suda, T., Matsuzaw, Y., Tani, H., 2009. Two-stage dual fluidized bed gasification: its conception and application to biomass. *Fuel Process. Technol.* 90, 137–144. <https://doi.org/10.1016/j.fuproc.2008.08.007>.
- Yang, H., Yue, G., Xiao, X., Lu, J., Liu, Q., 2005. 1D modeling on the material balance in CFB boiler. *Chem. Eng. Sci.* 60, 5603–5611. <https://doi.org/10.1016/j.ces.2005.04.081>.
- Yates, J.G., Lettieri, P., 2016. Effect of process conditions on fluidization. In: Yates, J.G., Lettieri, P. (Eds.), *Fluidized-Bed Reactors: Processes and Operating Conditions*. Springer International Publishing, Cham, pp. 137–173. https://doi.org/10.1007/978-3-319-39593-7_5.
- Youn, P.S., Lee, D.H., Kim, D., Won, Y.S., Choi, J.H., Joo, J.B., Ryu, H.J., 2022. Solids inventory and external solids circulation rate in risers of circulating fluidized beds. *Adv. Powder Technol.* 33. <https://doi.org/10.1016/j.apt.2022.103810>.
- F.A. Zenz, D.F. Othmer, Fluidization and fluid-particle systems, in: 1960. <https://api.semanticscholar.org/CorpusID:93826163>.
- Zhang, W., Johnsson, F., Leckner, B., 1995. Fluid-dynamic boundary layers in CFB boilers. *Chem. Eng. Sci.* 50, 201–210. [https://doi.org/10.1016/0009-2509\(94\)00222-D](https://doi.org/10.1016/0009-2509(94)00222-D).